AD-A150 254 VERTICAL DISCRIMINATION IN THE SOUND CHANNEL(U) MITRE 1/1
CORP MCLEAN VA S M FLATTE JAN 85 JSR-83-216
F19628-84-C-0001

UNCLASSIFIED F/G 20/1 NL

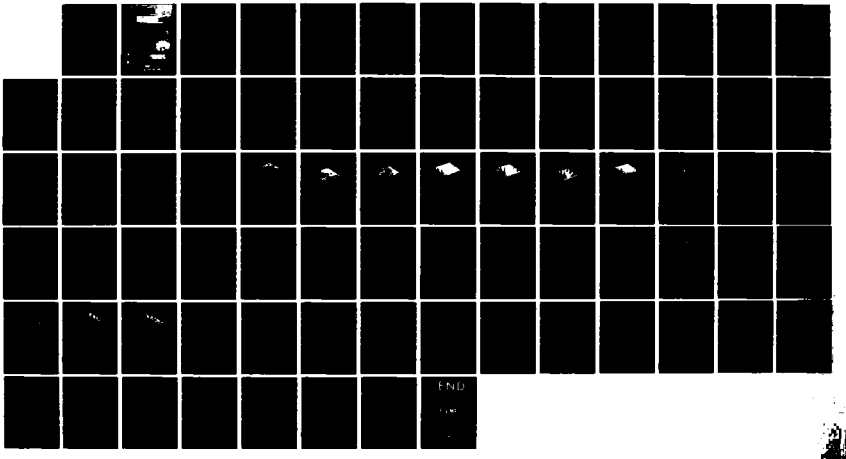

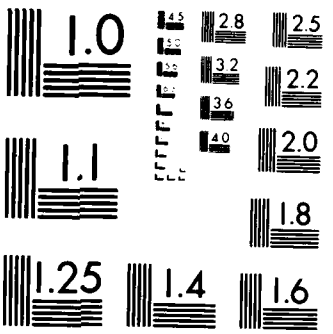

JASON

# Vertical Discrimination in the Sound Channel

Stanley M. Flatte

January 1985

JSR-83-216





JASON
The MITRE Corporation
1820 Dolley Madison Boulevard
McLean, Virginia 22102

UNCLASSIFIED

SECURITY CLASSIFICATION OF THIS PAGE (When Data Entered)

| REPORT DOCUMENTATION PAGE | | READ INSTRUCTIONS BEFORE COMPLETING FORM |
|---|---|---|
| 1. REPORT NUMBER<br>JSR-83-216 | 2. GOVT ACCESSION NO.<br>AD-A150 254 | 3. RECIPIENT'S CATALOG NUMBER |
| 4. TITLE (and Subtitle)<br>Vertical Discrimination in the Sound Channel | | 5. TYPE OF REPORT & PERIOD COVERED<br>6. PERFORMING ORG. REPORT NUMBER |
| 7. AUTHOR(s)<br>Stanley M. Flatté | | 8. CONTRACT OR GRANT NUMBER(s)<br>F19628-84-C-0001 |
| 9. PERFORMING ORGANIZATION NAME AND ADDRESS<br>The MITRE Corporation<br>1820 Dolley Madison Blvd.<br>McLean, VA 22102 | | 10. PROGRAM ELEMENT, PROJECT, TASK AREA & WORK UNIT NUMBERS |
| 11. CONTROLLING OFFICE NAME AND ADDRESS | | 12. REPORT DATE<br>~~July 1984~~ JAN. 1985<br>13. NUMBER OF PAGES<br>75 |
| 14. MONITORING AGENCY NAME & ADDRESS(if different from Controlling Office) | | 15. SECURITY CLASS. (of this report)<br>Uncl.<br>15a. DECLASSIFICATION/DOWNGRADING SCHEDULE |

16. DISTRIBUTION STATEMENT (of this Report)

DISTRIBUTION STATEMENT A
Approved for public release
Distribution Unlimited

17. DISTRIBUTION STATEMENT (of the abstract entered in Block 20, if different from Report)

18. SUPPLEMENTARY NOTES

19. KEY WORDS (Continue on reverse side if necessary and identify by block number)
Acoustics,
Vertical Arrays,
Vertical Discrimination,
Sound Channel..

20. ABSTRACT (Continue on reverse side if necessary and identify by block number)
This report describes the theory underlying vertical discrimination for vertical arrays on the sound-channel axis. It presents full wave-propagation calculations, incluing diffractive effects in the parabolic approximation, that quantiatively predict the behavior of finite arrays, even near caustics. These results confirm experimental observations and provide a single, approximate rule for the length of a vertical array necessary to distinguish between two acoutic sources. The formula is independent of range.

DD FORM 1 JAN 73 1473 EDITION OF 1 NOV 65 IS OBSOLETE

Uncl.

SECURITY CLASSIFICATION OF THIS PAGE (When Data Entered)

TABLE OF CONTENTS



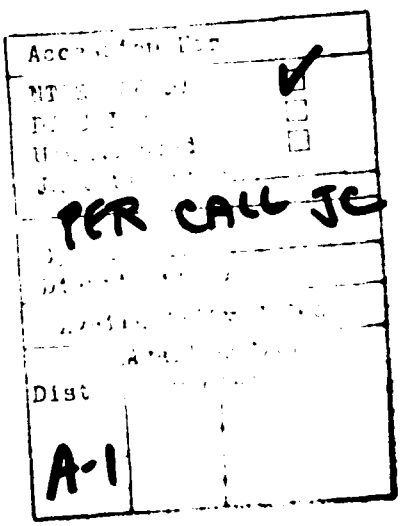

LIST OF ILLUSTRATIONS

## 1.0 INTRODUCTION

The ability to discriminate at long range between sound sources that are at different ocean depths would be useful for a variety of purposes. Ocean-acoustic experiments, underwater communication, and acoustic detection of submarines often suffer from background noise originating at the ocean surface, either from surface waves or from surface ships. If an acoustic source, whose purpose may be either ocean monitoring or cummunication, can be located several hundred meters below the surface, then a vertical array might be used to discriminate against unwanted noise.

A naive investigator might argue against the possibility of such vertical discrimination. The argument goes as follows: We are interested only in long-range systems (say 500 km as an example), which restricts us to low frequencies (say 150 Hz as an example) because of absorption. A simple calculation of the resolution of an array would say that to distinguish two sources separated by 50 m at 1000 km range would require a 200-km-long vertical array. Since the depth of the ocean is less than 5 km, the task is impossible.

Yet, several experiments by Fisher and Williams[1,2] using a vertical array at the depth of the sound channel axis have indicated a substantial difference in vertical arrival angle of the energy

arriving from two sources at depths of 25 and 80 meters. These differences persist out to ranges of 1500 kilometers and possibly more.

Although simple ray-tracing arguments support the experimental results, the validity of ray tracing at 150 Hz to ranges greater than 1000 km is open to question.

It is the purpose of this note to present full wave-propagation calculations, including diffractive effects in the parabolic approximation, that quantitatively predict the behavior of finite arrays, even near caustics. The results confirm the experimental observations, and provide a simple way to predict results for a variety of sound channels. The calculations were carried out with parabolic-equation numerical simulation.

A simple approximate rule for vertical discrimination can be given as follows: The approximate length, $D$, of a vertical array necessary to distinguish between two acoustic sources is

$$D = \frac{600 \text{ m}}{\Delta T} \left(\frac{150 \text{ Hz}}{f}\right) \qquad (1)$$

where $f$ is the acoustic frequency and $\Delta T$ is the temperature difference between the two source depths. For example, the CONTRK

experiment had a temperature difference of about 4 $^{o}$C between their 25 m and 80 m source depths, so would only have required a 150-m array to resolve at 150 Hz. Since they had a 500 m array, they did well. The important point is that (1) shows no dependence on range. It doesn't matter how far away the array is from the source; the vertical discrimination is undiminished. Thus the presence of the sound channel completely invalidates the naive array-resolution argument at long range.

The above rule applies to vertical arrays on the sound-channel axis. Calculations indicate that putting an array at the reciprocal depth of one of the sources gives very poor discrimination against a source at another depth.

## 2.0 EXPERIMENT DESCRIPTION

Both in 1977 and 1979 a vertical array was hung from FLIP a few hundred miles off San Diego, California. The configuration is shown if Figure 1. The acoustic sources were hung from the R/V NEW HORIZON, which steamed at about six knots from FLIP is a northwesterly direction (Figure 2).

The raytrace for acoustic energy from the 80-m source is shown in Figure 3, illustrating the dependence of the peak arrival angle as a function of range, including shadow zones which occur out to approximately zone 5. Some experimental results that verify the features of Figure 3 are shown in Figure 4. More detailed angular distributions as a function of range are shown in Figure 5. The energy arriving at the array is shown on a linear scale.

Plots of the angular distribution averaged over range at long range are shown in Figures 6 and 7 for the 25 m and 80 m deep sources, respectively. It is the difference between Figures 6 and 7 that we would like to confirm theoretically.

Finally, it will be useful to have the angular distribution of ambient noise in the ocean at the time of this experiment.

Figure 8 shows that the energy is arriving more or less uniformly between $-16^{o}$ and $+16^{o}$.

## 3.0 PARABOLIC-EQUATION PRINCIPLES

It is known that at 150 Hz the propagation of sound in the ocean volume is controlled by the wave-speed (index-of-refraction) variations that occur due to temperature, salinity, or pressure difference in the water. The most pronounced of these effects is the sound channel itself, which has vertical scales of variation of hundreds of meters. If the scales of variation are large compared with a wavelength, then the sound is deviated from its original direction by only a small angle. Energy within the sound channel occupies a vertical-angle region within $\pm 15^{\circ}$ from the horizontal; other angles are absorbed in the ocean bottom.

Under these conditions of small-angle deviation, the sound propagation obeys a parabolic approximation to the full wave equation. This approximation is of the form

$$-\frac{1}{2q}\,\partial_{zz}\Psi + q\mu(z)\Psi = i\partial_x\Psi \qquad (2)$$

where $\Psi(x,z)$ is the demodulated sound amplitude; $x$ is the range; $z$ is the depth, $q$ is the acoustic wavenumber, and $\mu(z)$ is the fractional deviation of sound speed from the reference value used to calculate $q$ .

The boundary condition at the ocean surface is a pressure-release reflection

$$\Psi(x,0) = 0 \tag{3}$$

and the boundary condition at the ocean bottom is that $\Psi(x, -h)$ be only an outgoing wave; that is, a perfectly absorbing ocean bottom at depth $h$ .

The initial wave at $x = 0$ can be adjusted to give an approximation to whatever the source may be: for example, a point source.

The computer realization of the PE method in our code is a split-step Fast Fourier Transform.

$$\Psi(x+dx,z) = \exp\left[\tfrac{1}{2}\, iAdx\right] \exp\left[iBdx\right] \exp\left[\tfrac{1}{2}\, iAdx\right] \Psi(x,z) \tag{4}$$

$$A = \frac{1}{2q}\, \partial_{zz} \tag{5}$$

$$B = -q\mu(z) \tag{6}$$

and the evaluation of the exponential of the second derivative is carried out by FFT:

$$\exp[iAdx]\phi(z) = F^{-1}\{\exp[i\tilde{A}dx]\ F[\phi(z)]\ \} \tag{7}$$

$$\tilde{A} = -\frac{1}{2q}\,k^2 \tag{8}$$

where F stands for Fourier transform from z-space to k-space.

The surface boundary condition is treated by doubling the depth region and introducing a reflected source $\Psi(0,-z)$ above the ocean surface.

The bottom is treated by multiplying each $\Psi(x,z)$ by a depth-dependent absorption factor

$$L(z) = \exp\{-\alpha\ dx\ \exp[\ (\frac{z-h}{\beta})^2]\ \} \tag{9}$$

where our runs have used $\alpha = 0.05\ m^{-1}$ , $\beta = 0.04\ h$ , and $h = 5120$ m. This allows energy above a depth of a bit more than 4 km to be unaffected by the bottom, yet gives very little reflection from the bottom.

The FFT is carried out with 512 points over the "real" ocean; that is a total 1024-point transform when the reflected ocean

is included. The step size in range at 150 Hz has been taken as 0.5 km.

The initial wavefunction $\Psi(0,z)$ is

$$\Psi(0,z) = 0.9144(\pi\lambda)^{-1/2}\{\exp[-(\frac{z-z_s}{\lambda})^2\ ] - \exp[-(\frac{z+z_s}{\lambda})\ ]\ \} \qquad (10)$$

where $\lambda$ is the acoustic wavelength. This form closely approximates a point source at depth $z_s$ with unit intensity at a range of one yard.

The intensity of the wave at range $x$ is then

$$I(x,z) = \frac{|\Psi(x,z)|^2}{x} \qquad (11)$$

## 4.0 PARABOLIC-EQUATION SIMULATION RESULTS

The detailed sound-speed profile used in the PE simulations was obtained from Bruce Williams as representative of the 1979 CONTRK V experiment (Figure 9). Three source depths were chosen: 25 m, 80 m, and 150 m. It is seen in Figure 9 that the reciprocal depths for these sources are 3800 m, 2800 m, and 1900 m, respectively.

The computer-simulated data were analyzed in terms of 500-m-long arrays placed at two depths; the first, from 500-1000 m, simulated the CONTRK V experiment; the second, from 3500-4000 m, simulated a reciprocal-depth experiment. The computer was run out to a range of 1300 km, and data was kept from 10-300 km and from 1000-1300 km in one kilometer steps.

### 4.1 Intensity as a Function of Range and Depth

Figures 10-12 show $|\psi|^2$ on a linear scale as a function of range and depth. The first convergence zone at 50-60 km is seen clearly, as is the absorbing bottom. The traces of convergence zones at 1000 km are seen for the 150-m-deep source, but not for the 25-m-deep source. These figures gives confidence that the code is functioning properly.

## 4.2 Intensity as a Function of Range and Angle with an Axis Array

Figures 13-18 show $|\Psi|^2$ on a linear scale as a function of range and vertical angle, where zero degrees is the horizontal direction. The array is at 500-1000 m depth, straddling the sound axis.

At short range the convergence zones are seen clearly, and the difference between the angles received from the different sources are also seen clearly, with the shallower sources giving steeper angles.

At long range the angle differences persist, even when the vestiges of convergence zones completely disappear. It is noteworthy that the deeper (150 m) source still has clearly defined convergence zones even at 1200 km range. The steep thermocline breaks up long-range convergence zones for sources within it, but sources below it will still have strong convergence zones beyond 1000 km.

The angular distributions, averaged over two-hundred-kilometer range increments, are shown in Figures 19-24. No significant differences between the distributions at 0-200 km and those at 1000-1200 km are seen, but the difference in angles for sources at different depths is striking, These plots can

be compared with the experimental data in Figures 6 and 7. The comparison is quite good.

The distribution of intensity versus range, averaged over all vertical angles, but using the axis array, is shown in Figures 25-30. At short range the convergence zones are so marked that detection within the shadow zones is likely to be difficult. At long range, the energy from relatively shallow sources is spread more or less uniformly, so that gaps in detection will not occur. However the 150-m source still shows strong convergence zones at 1200 km, as remarked previously.

### 4.3 Intensity as a Function of Range and Angle with a Reciprocal-Depth Array

It has been suggested that an array at the reciprocal depth for a given source may have good discrimination against other sources. The reciprocal depth is that depth that has the same sound speed as the source depth. Thus a ray leaving the source with zero angle will approach the reciprocal depth at zero angle.

Figures 31-36 show the intensity as a function of range and vertical angle inpinging on an array at 3500-4000 depth, which is approximately the reciprocal depth of a 25 m source. Convergence zones at short range are seen, and differences in arrival-angle distributions for different sources are seen, but the fundamental

fact is that the energy from all the shallow depths is concentrated within $5^{o}$ of zero angle, so that discrimination of source depth is practically nonexistent. Without a doubt the axis array has better discrimination.

The distributions in vertical angle averaged over range are shown in Figures 37-42 and the distributions in range averaged over vertical angle are shown in Figures 43-48.

## 5.0 CONCLUSIONS

The use of a vertical array on the axis to distinguish the depth of an acoustic source at long-range and low frequency is technically feasible. The discrimination power of the array depends on the shape of the sound-channel, and is independent of range to a good approximation. Parabolic-equation computer simulations of wave propagation at 150 Hz and 1300 km have confirmed an experimental result on this topic.

The full-wave propagation results indicate that a simple rule taken from ray tracing should be reasonably accurate; consider the energy emitted by an acoustic source to be primarily at zero vertical angle. Then the vertical angle at the sound channel axis can be calculated from the sound speed at the source depth and the sound speed at the axis, by Snell's Law. The difference between the axis angles of sources at two different depths is then

$$\theta_2^2 - \theta_1^2 = \frac{2}{C_o} \left( C(z_2) - C(z_1) \right) \qquad (12)$$

In the usual sound channel both $\theta_1$ and $\theta_2$ are abour $12^o$, and the difference $C(z_2) - C(z_1)$ is dominated by the temperature difference $\Delta T$ between the two depths. We have

$$C_o^{-1} \Delta C \approx \alpha \Delta T \tag{13}$$

where $\alpha = 3 \times 10^{-3}\ {}^{o}C^{-1}$ . The resolution of a vertical array length $D$ is $\lambda/D$ , so that the array length $D$ needed to resolve two sources can be derived:

$$D \approx \frac{\lambda\theta}{\alpha\Delta T} \tag{14}$$

For 150 Hz we have $\lambda = 10$ m . Taking $\theta \approx 0.2$ we have

$$D \approx \frac{600}{\Delta T} \tag{15}$$

Obviously two sources within the mixed layer will not be well discriminated. However any source in water a few degrees cooler than surface water should be well discriminated by a several-hundred-meter array.

A study of the depth at which the difference in sound-axis vertical angle with the surface-limited ray is equal to $1^{o}$ has been done by J. Lovett[3]. Figures 49 and 50 show the depth (in feet) at which this discrimination would be possible if the array were able to resolve a $1^{o}$ difference. The second number in each ocean region is the axis angle of the surface-limited ray.

As expected, those regions of the ocean with a sharp thremocline are able to discriminate smaller depth differences.

The use of a deep array (either moored or towed) does not look attractive for discrimination because all sources put a broad range of angles around zero degrees into such an array.

The signal-to-noise gain at 150 Hz with a 500 m vertical array can be calculated by comparing the width of the angular dist-ibution of received intensity, which appears to be about $2^{o}$, with the $\approx 30^{o}$ width for ambient noise. Thus the gain should be about 12 dB. It would be desirable to calculate this gain with various sound channels, and, at higher acoustic frequencies, with account taken of angular spread due to scattering from ocean fluctuations.

One difficulty with this axis array is that shadow zones are significant, either for short ranges or deep sources. A broad study of many realistic sound channels should be done to ascertain at what range the shadow zones fill in. This will depend on source depth. Also it would be desirable to develop an analytic approach beyond raytracing for this problem.

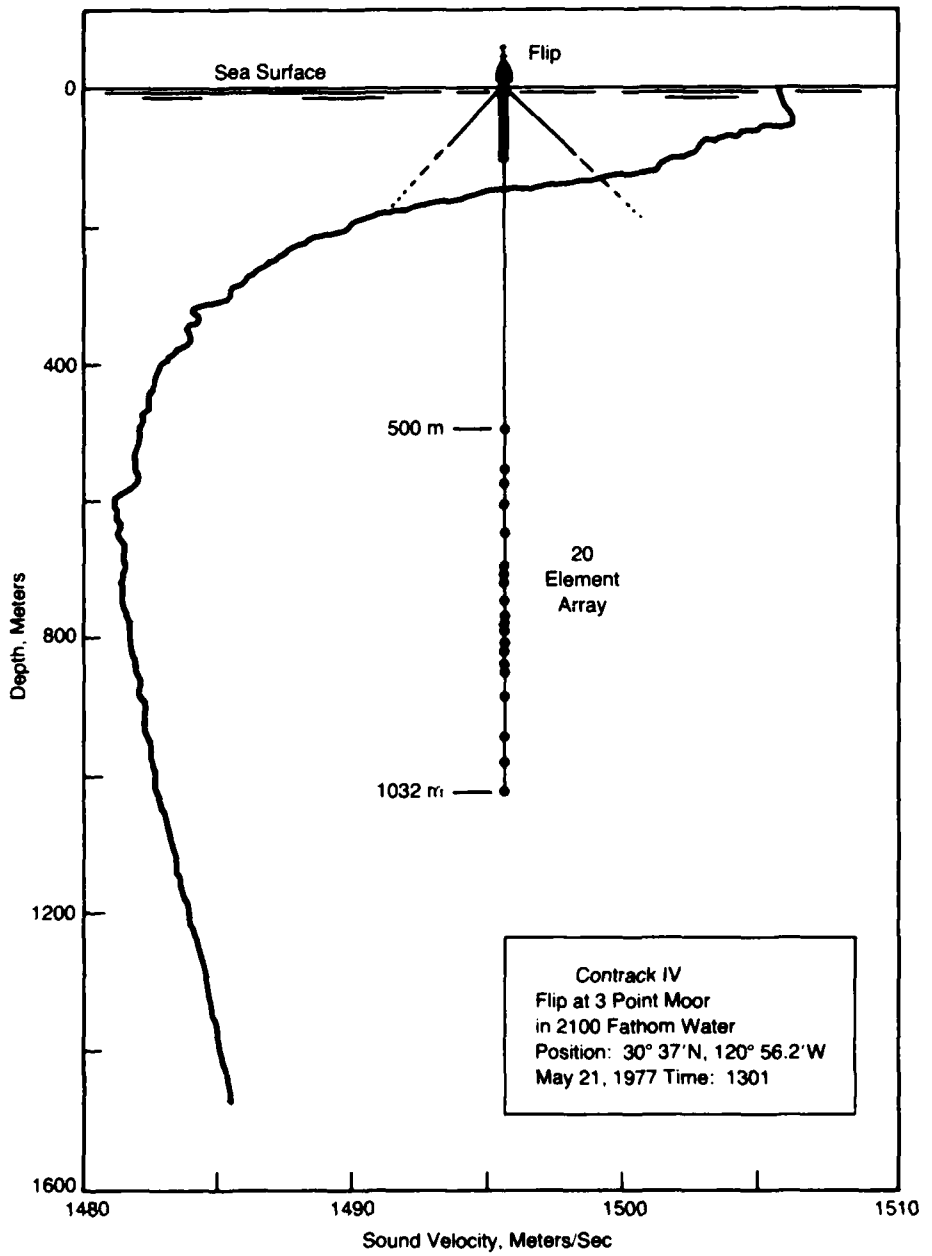


**Figure 1.** Configuration of CONTRK vertical array.

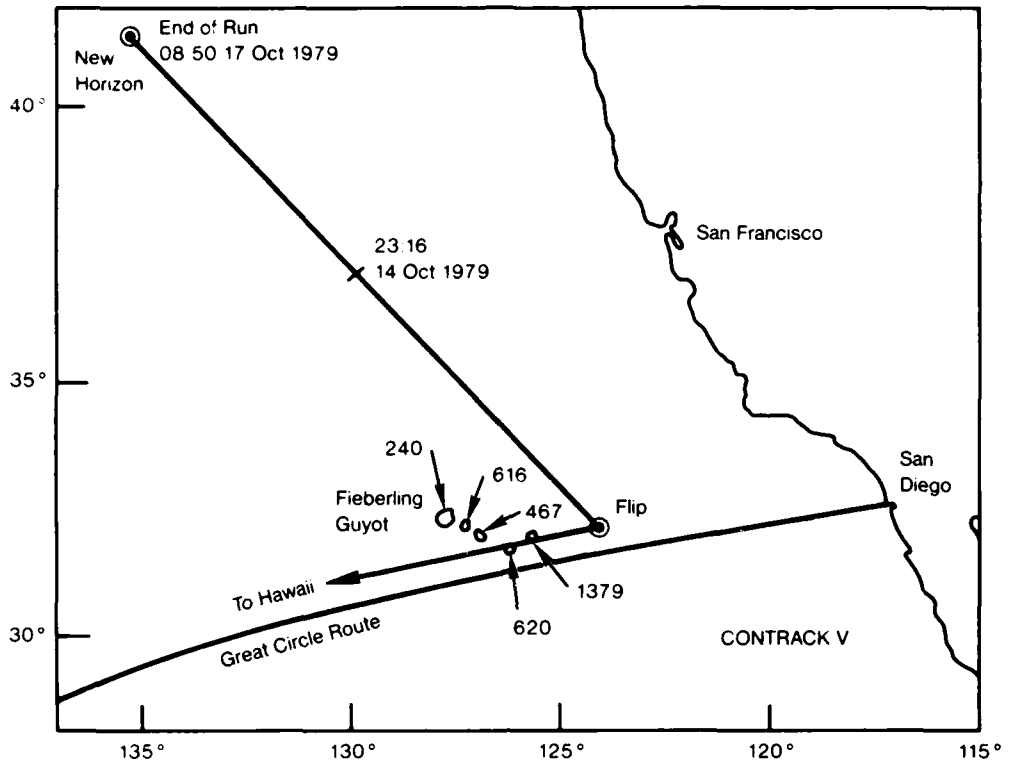


**Figure 2**. Path of New Horizon towing the acoustic source for CONTRK V.

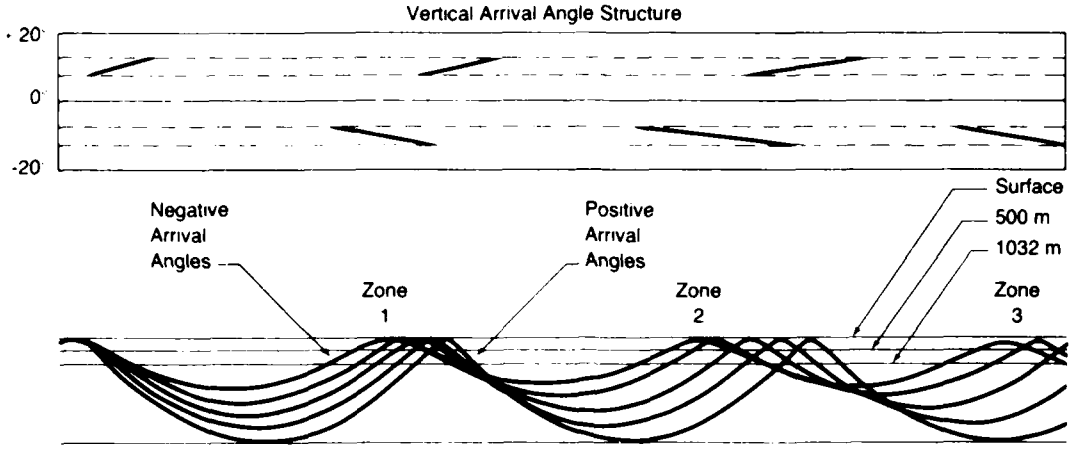


**Figure 3.** Raytrace for acoustic energy from the 80-m source.

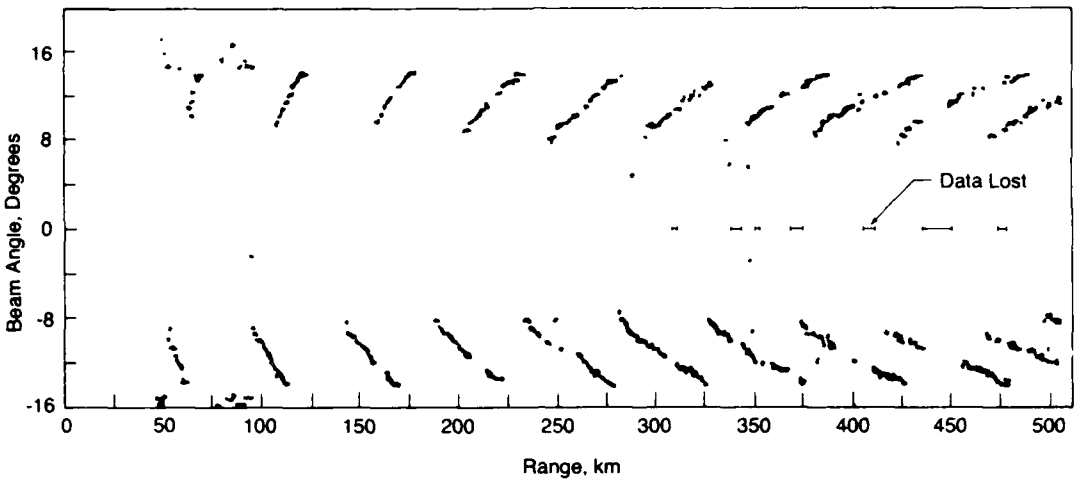


**Figure 4**. Angle of peak acoustic energy as a function of range.

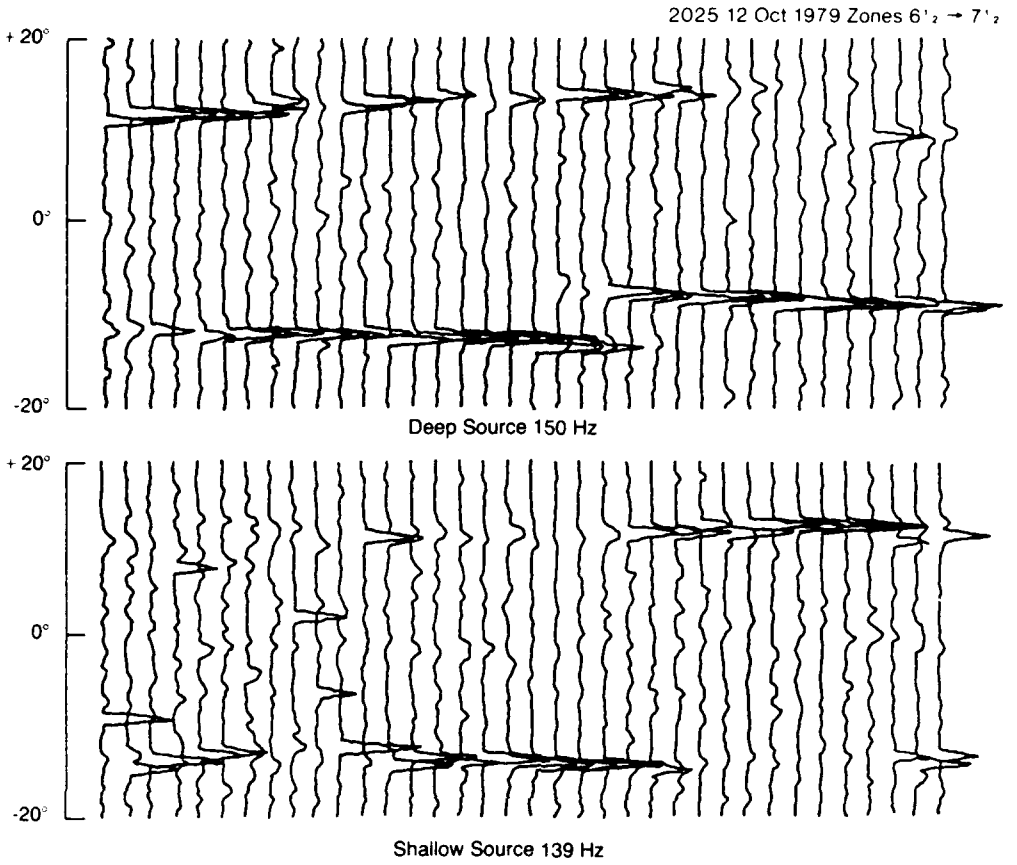


**Figure 5.** Received intensity as a function of vertical angle and elapsed time, detected by the vertical array.

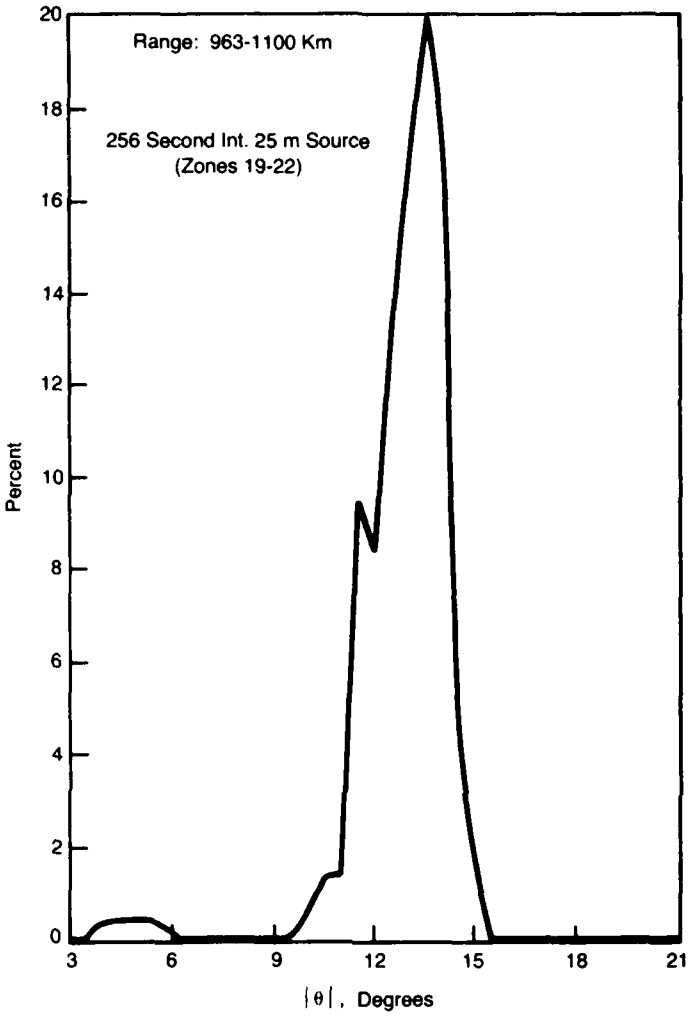


**Figure 6.** Angular distribution averaged over range at about 250 km for the 25-m-deep source.

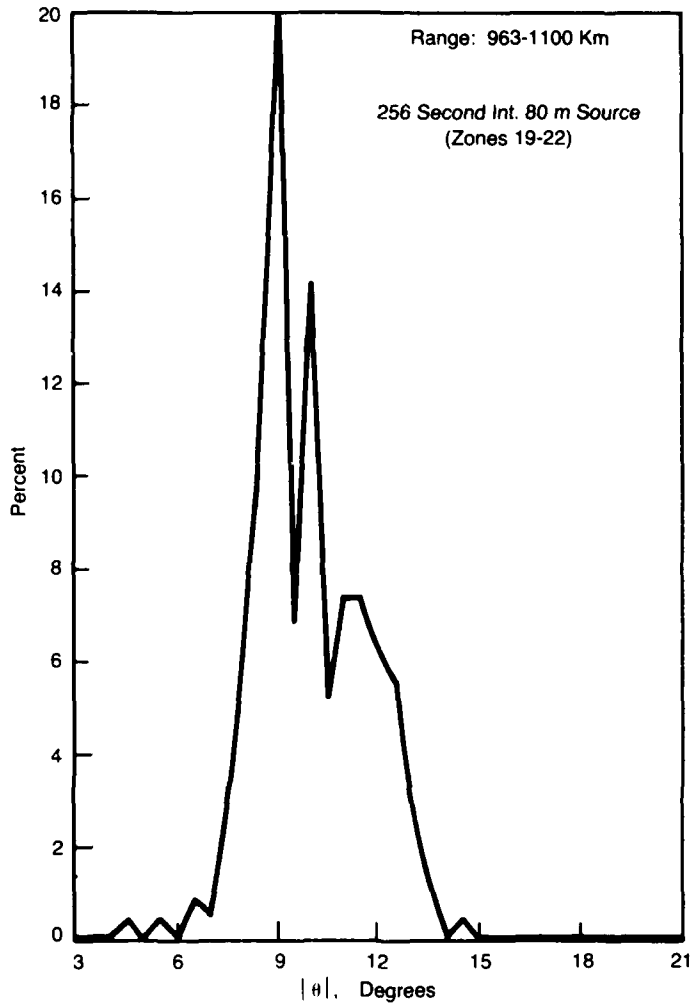


**Figure 7.** Angular distribution averaged over range at about 250 km for the 80-m-deep source.

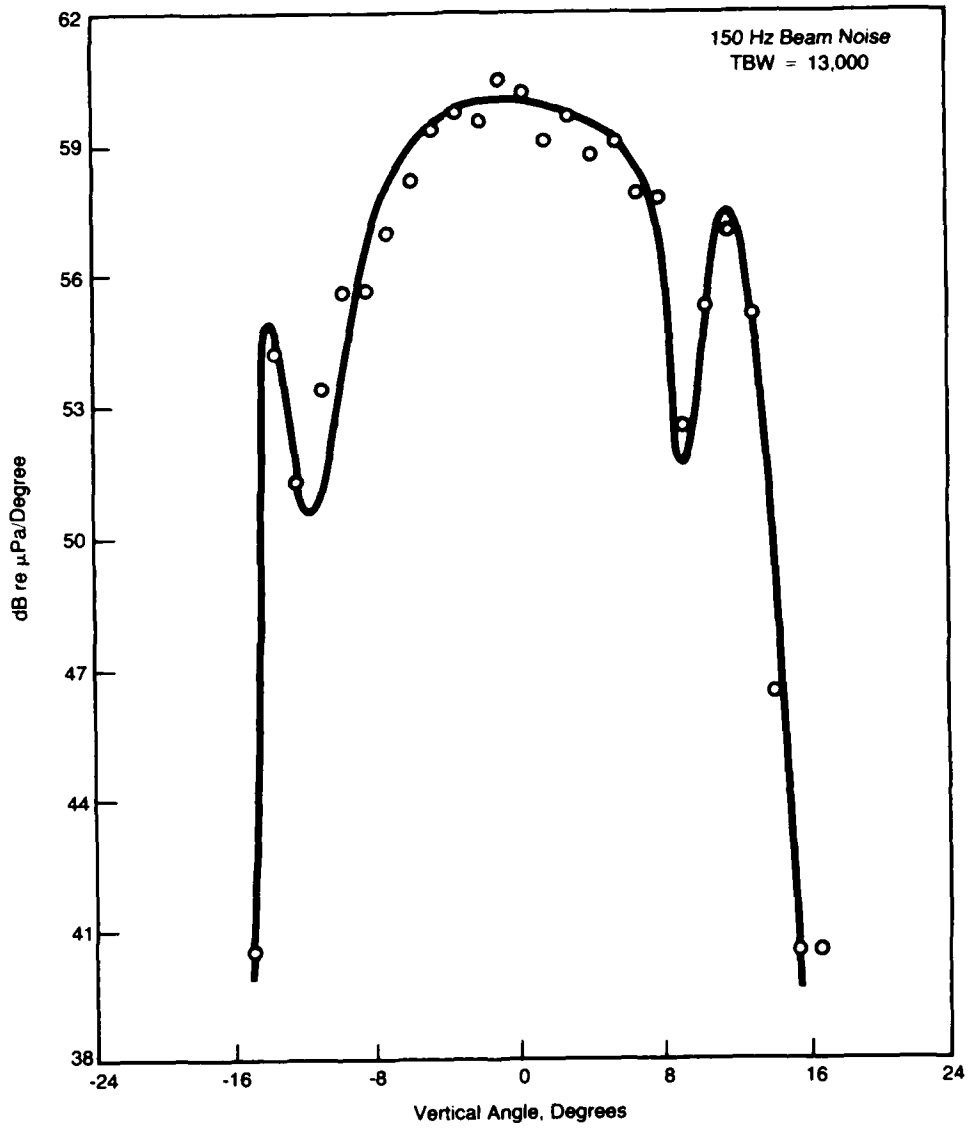


**Figure 8.** Ambient noise as a function of vertical angle.

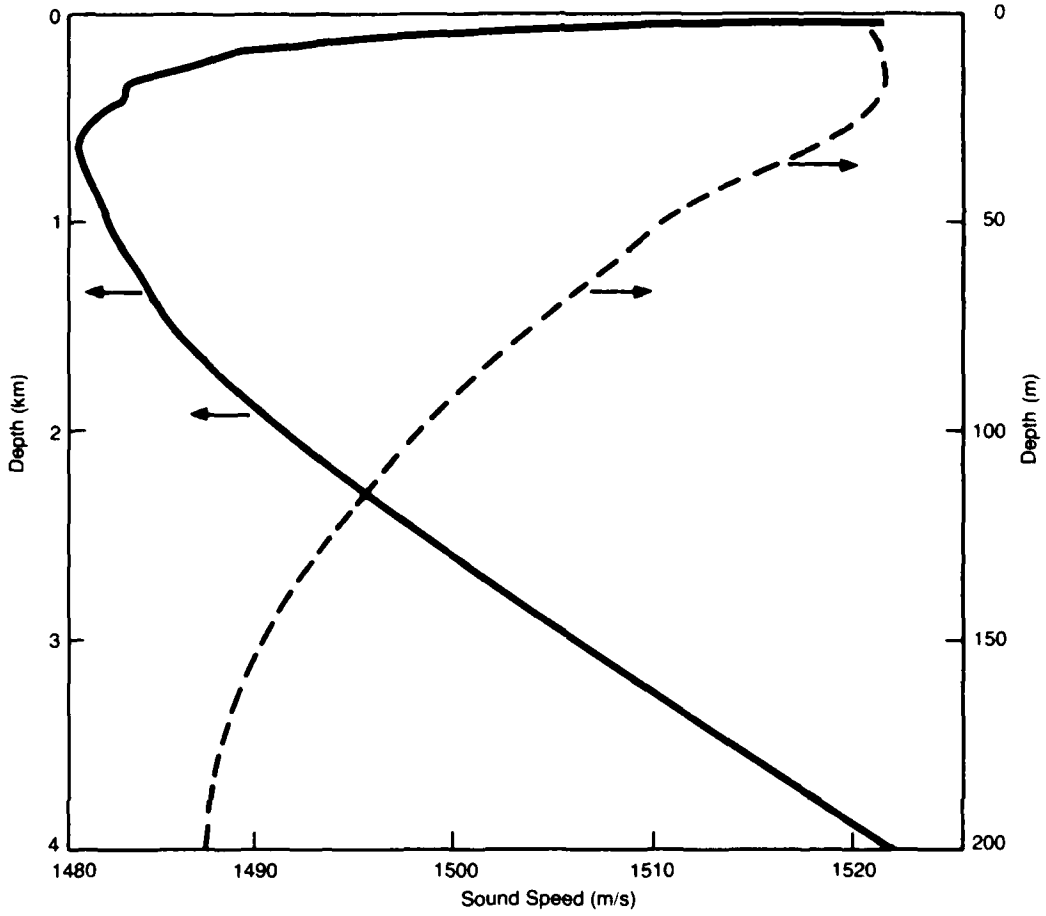


**Figure 9.** Sound speed profile for CONTRK V.

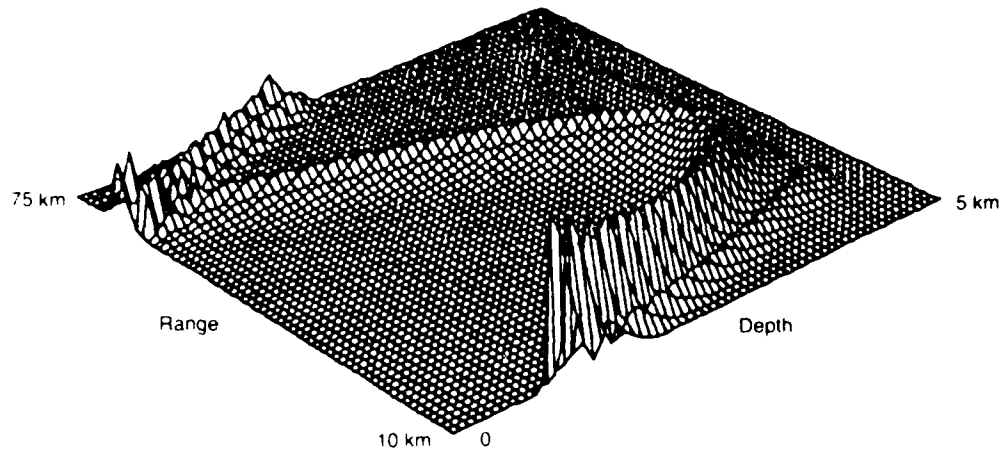


**Figure 10**. Intensity versus depth and range

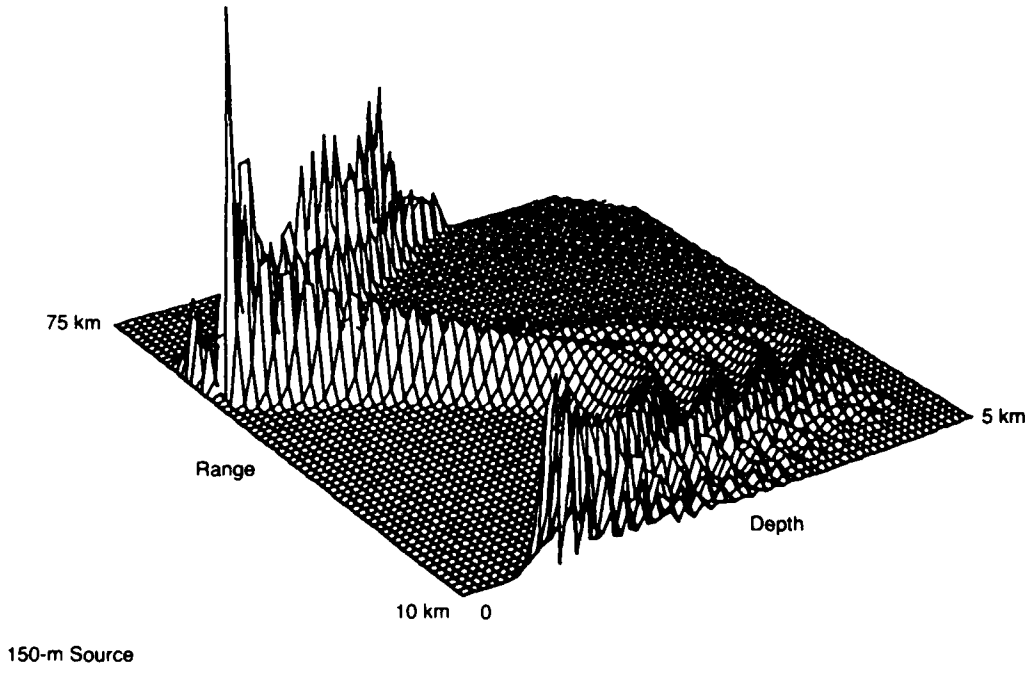


**Figure 11.** Intensity versus depth and range.

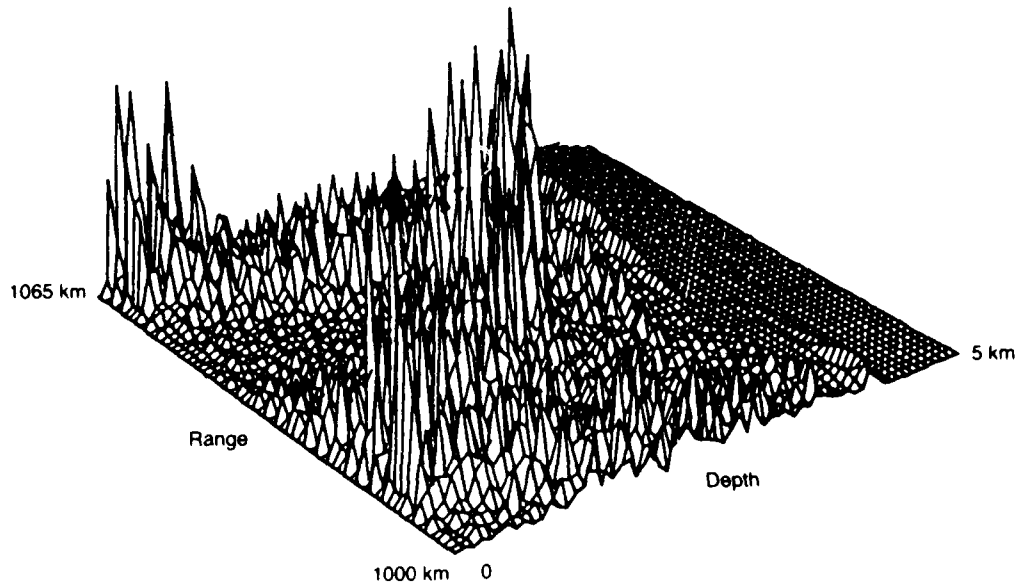


**Figure 12**. Intensity versus depth and range.

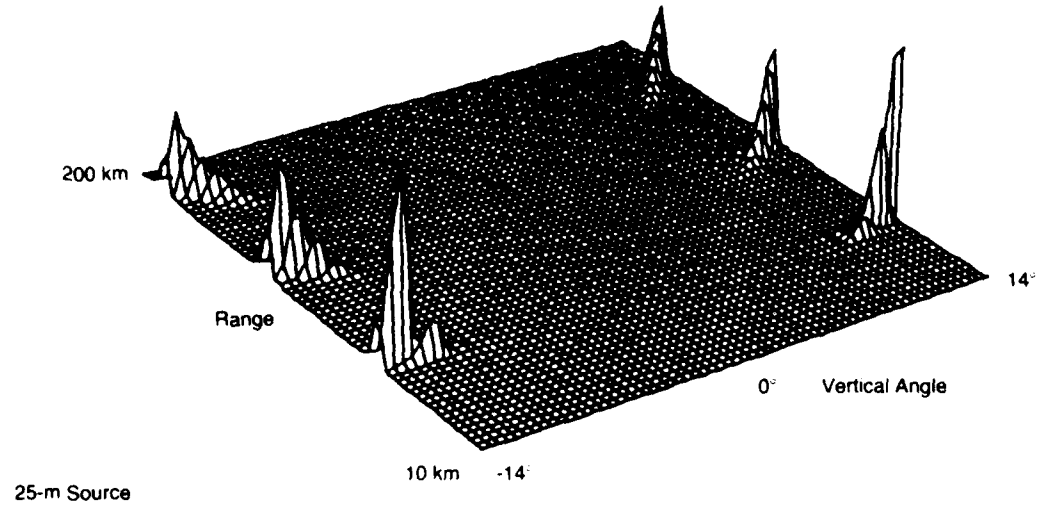


**Figure 13.** Information from a dense array between 500 and 1000 m depth.

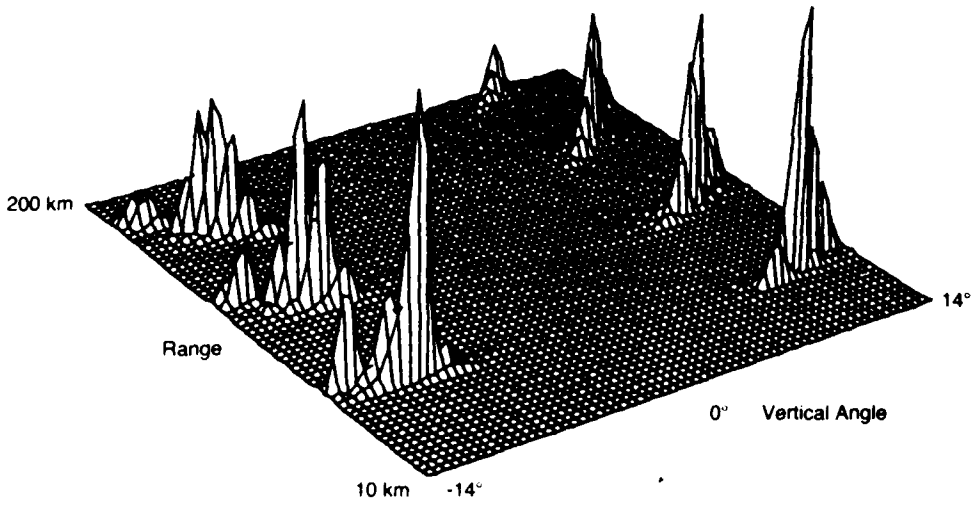


**Figure 14**. Information from a dense array between 500 and 1000 m depth.

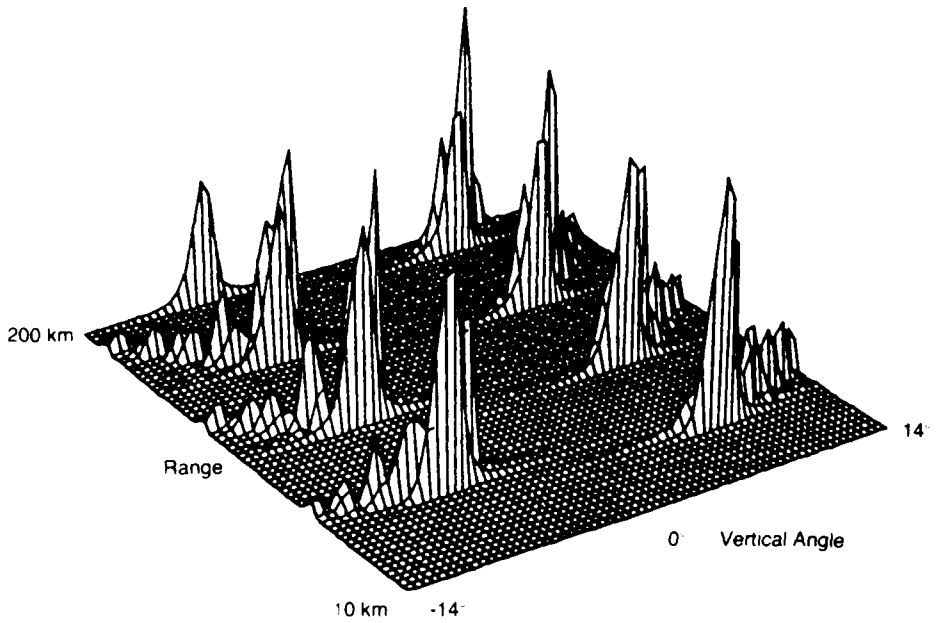


**Figure 15.** Information from a dense array between 500 and 1000 m depth.

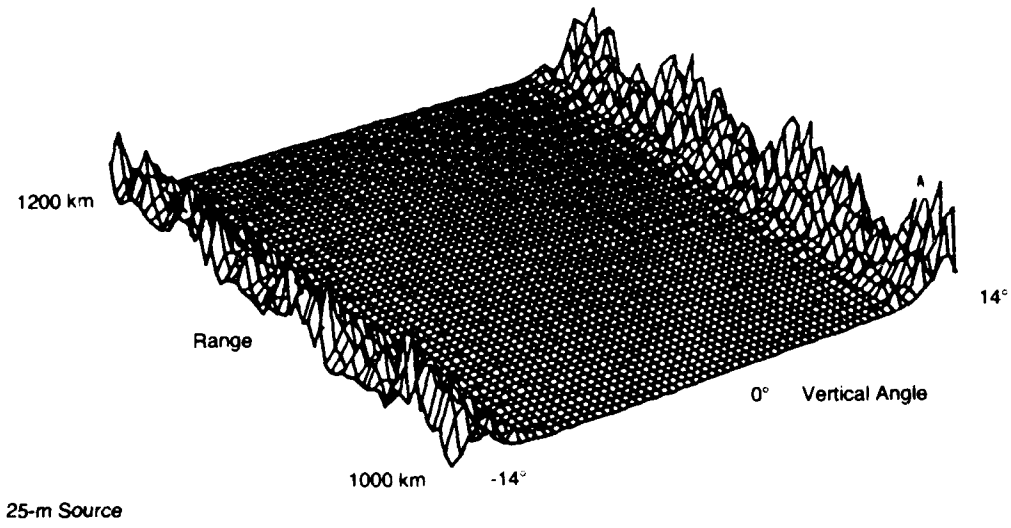


**Figure 16.** Information from a dense array between 500 and 1000 m depth.

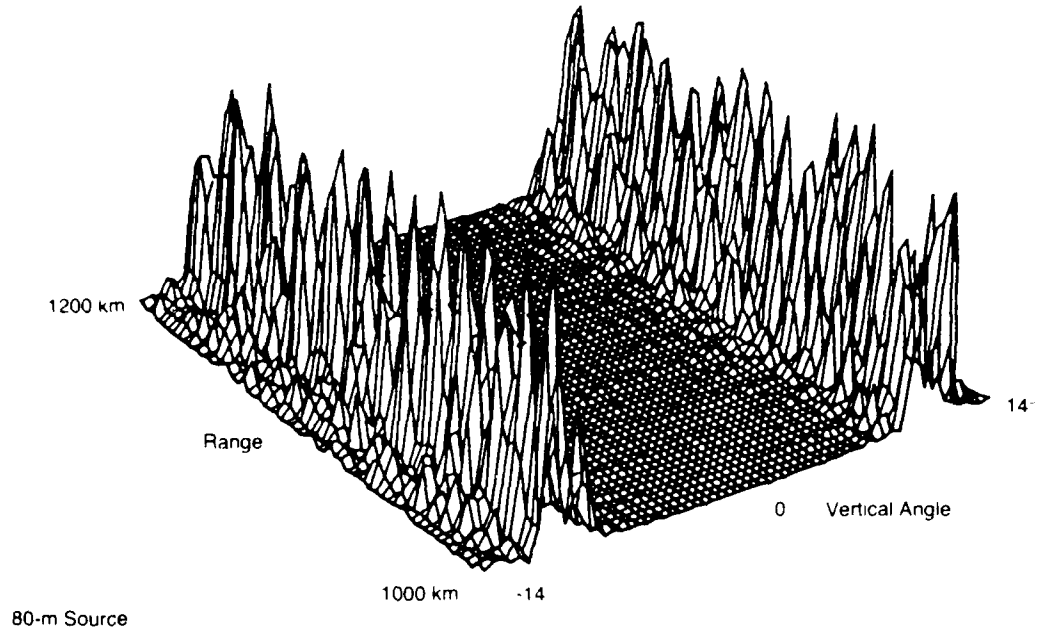


**Figure 17**. Information from a dense array between 500 and 1000 m depth.

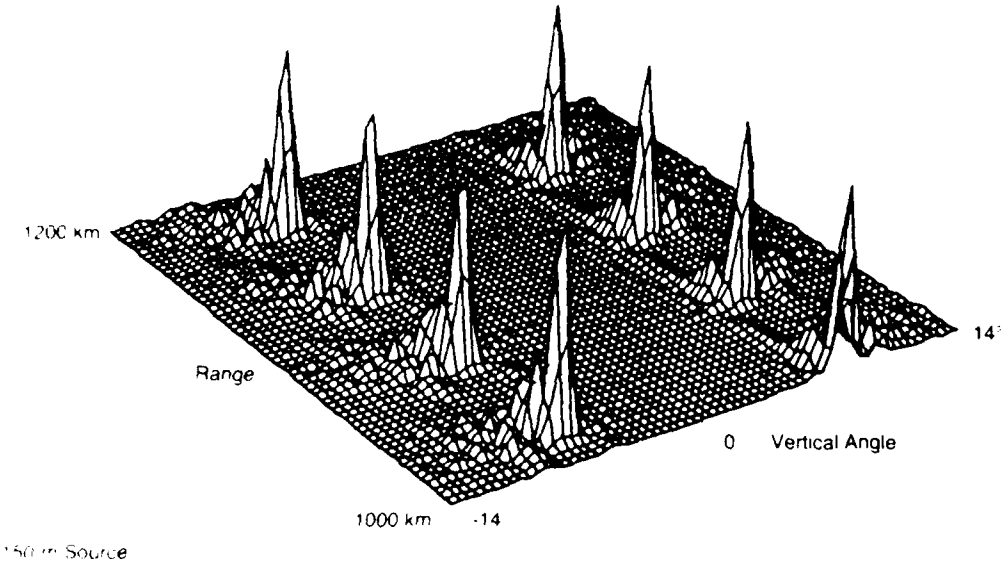


**Figure 18** Information from a dense array between 500 and 1000 m depth.

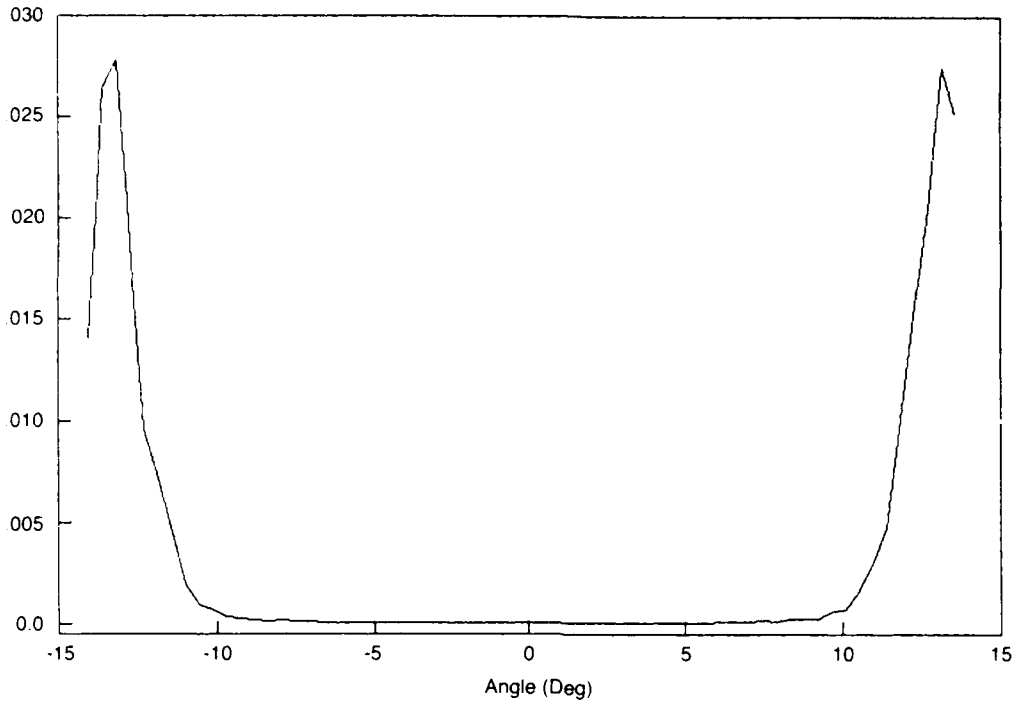


**Figure 19**. Information from a dense array between 500 and 1000 m depth.

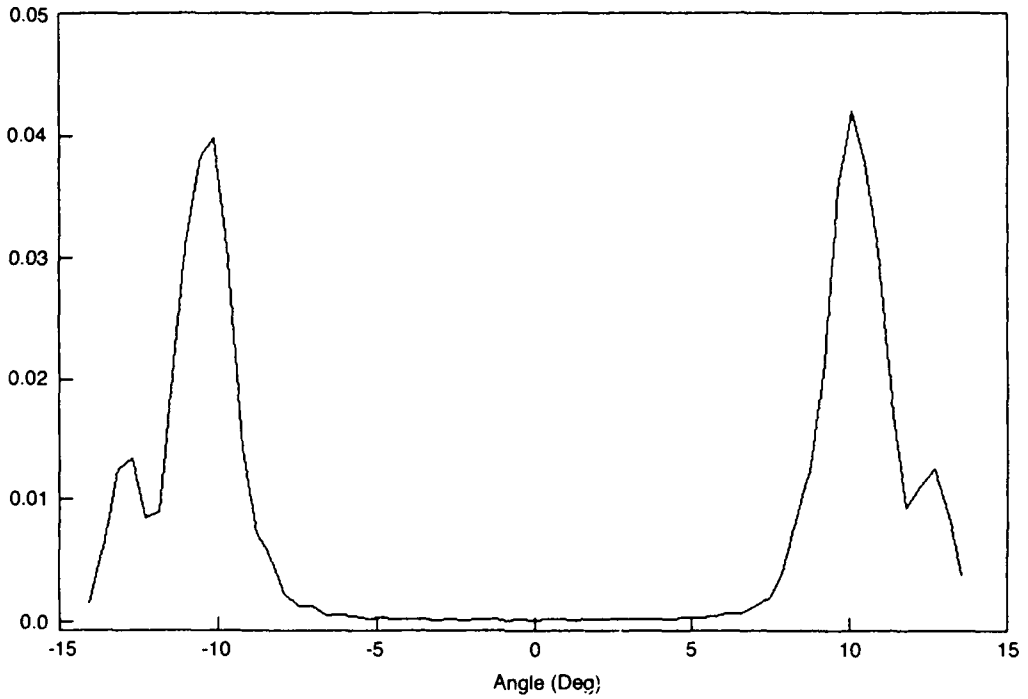


Source: 80 m; Short Range; Shallow Receiver

**Figure 20.** Information from a dense array between 500 and 1000 m depth.

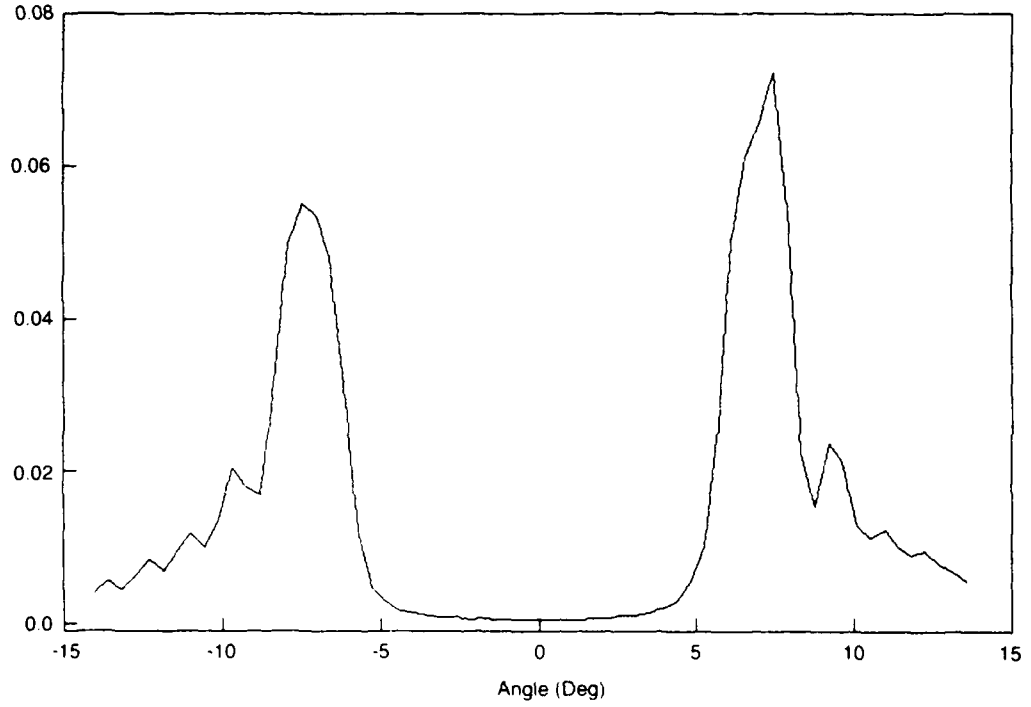


Source: 150 m; Short Range; Shallow Receiver

**Figure 21**. Information from a dense array between 500 and 1000 m depth.

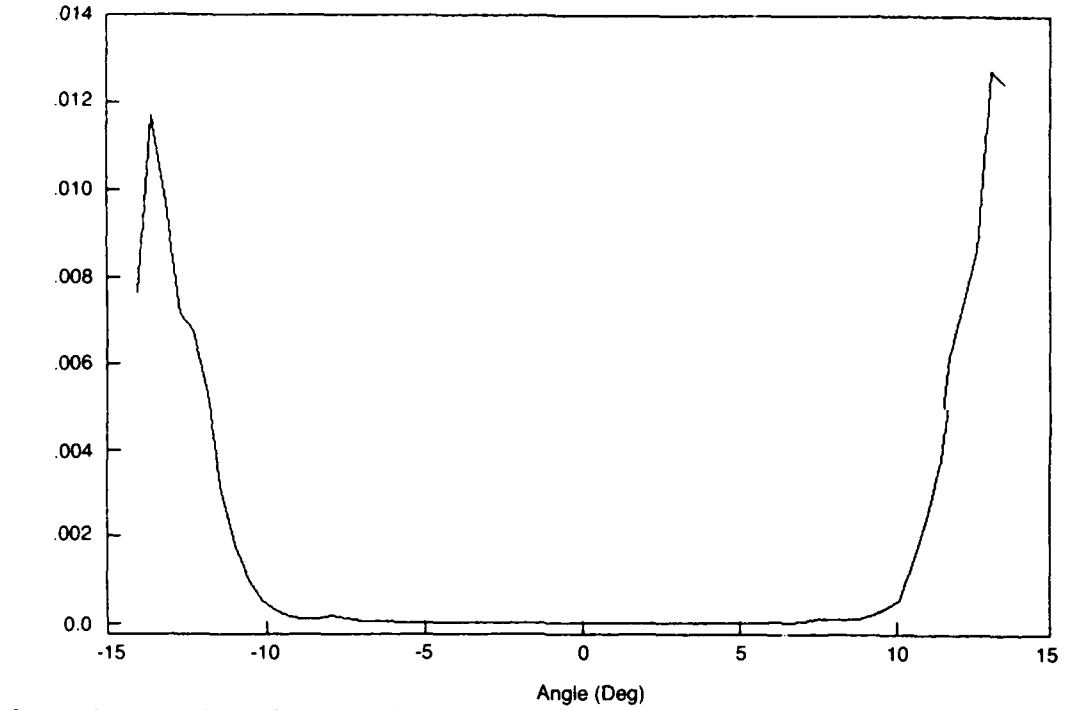


**Figure 22.** Information from a dense array between 500 and 1000 m depth.

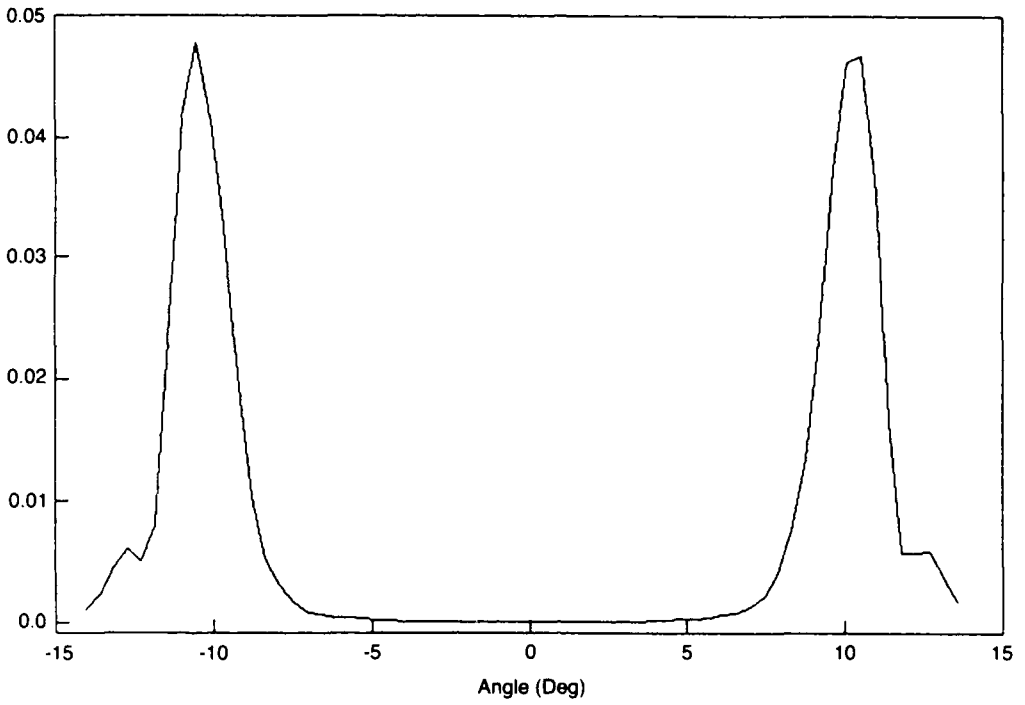


Source: 80 m; Long Range; Shallow Receiver

**Figure 23.** Information from a dense array between 500 and 1000 m depth.

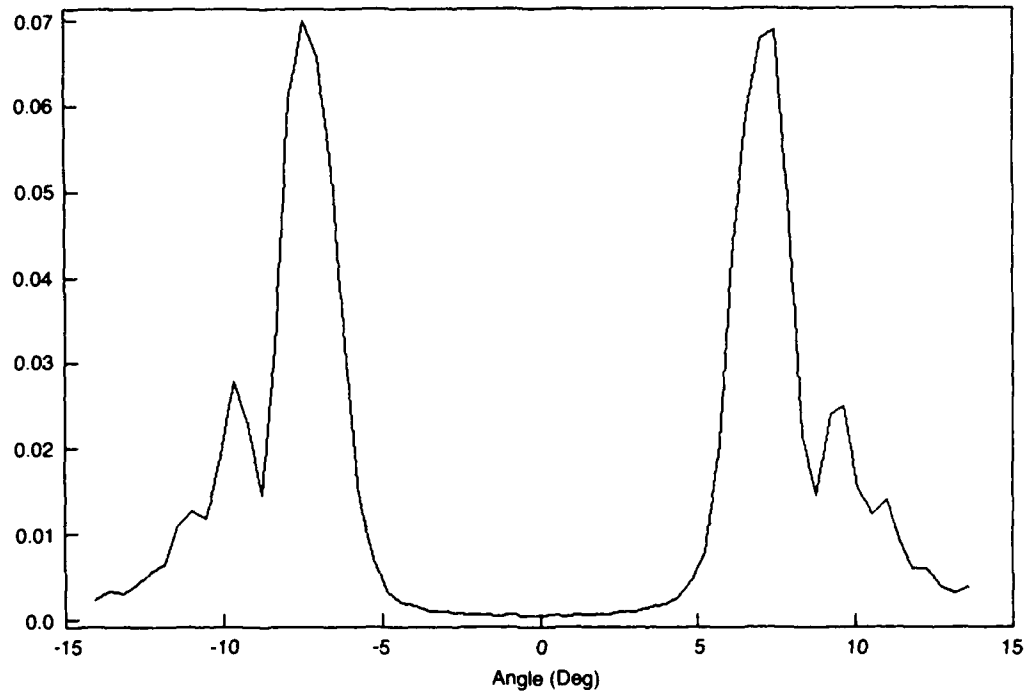


Source: 150 m; Long Range; Shallow Receiver

**Figure 24.** Information from a dense array between 500 and 1000 m depth.

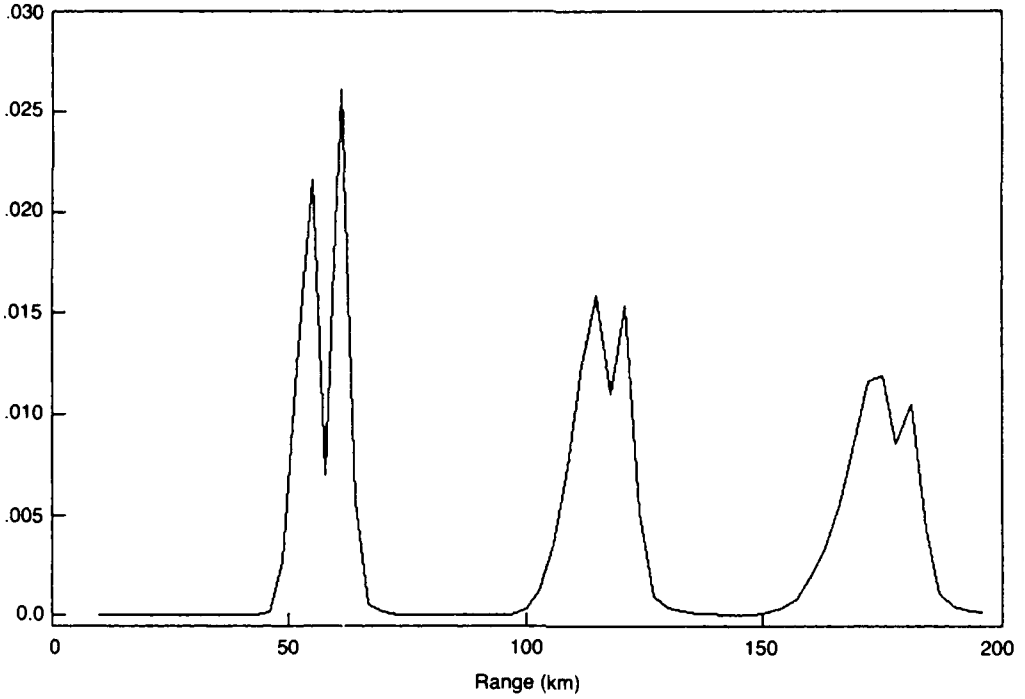


Source: 25 m; Short Range; Shallow Receiver

**Figure 25.** *Information from a dense array between* 500 *and* 1000 m depth.

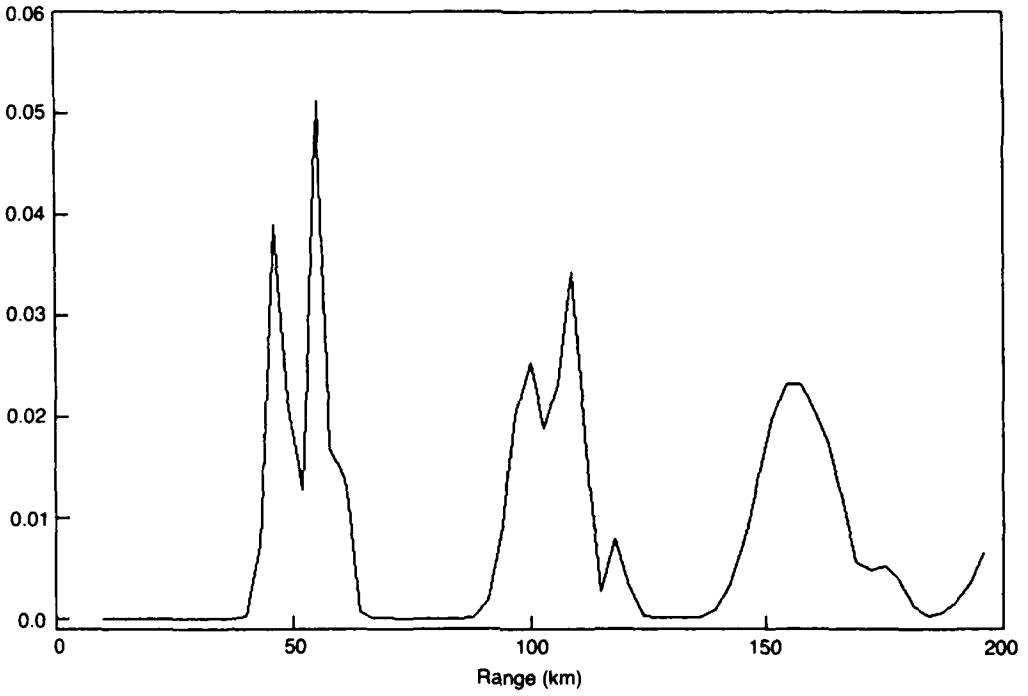


Source: 80 m; Short Range; Shallow Receiver

**Figure 26.** Information from a dense array between 500 and 1000 m depth.

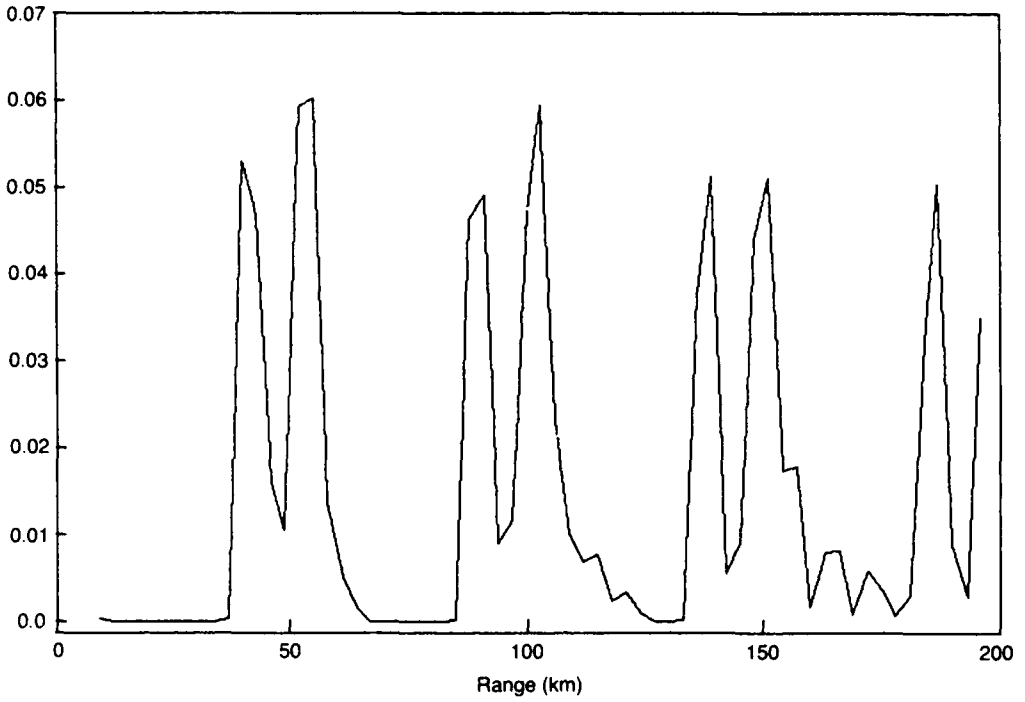


Source: 150 m; Short Range; Shallow Receiver

**Figure 27.** Information from a dense array between 500 and 1000 m depth.

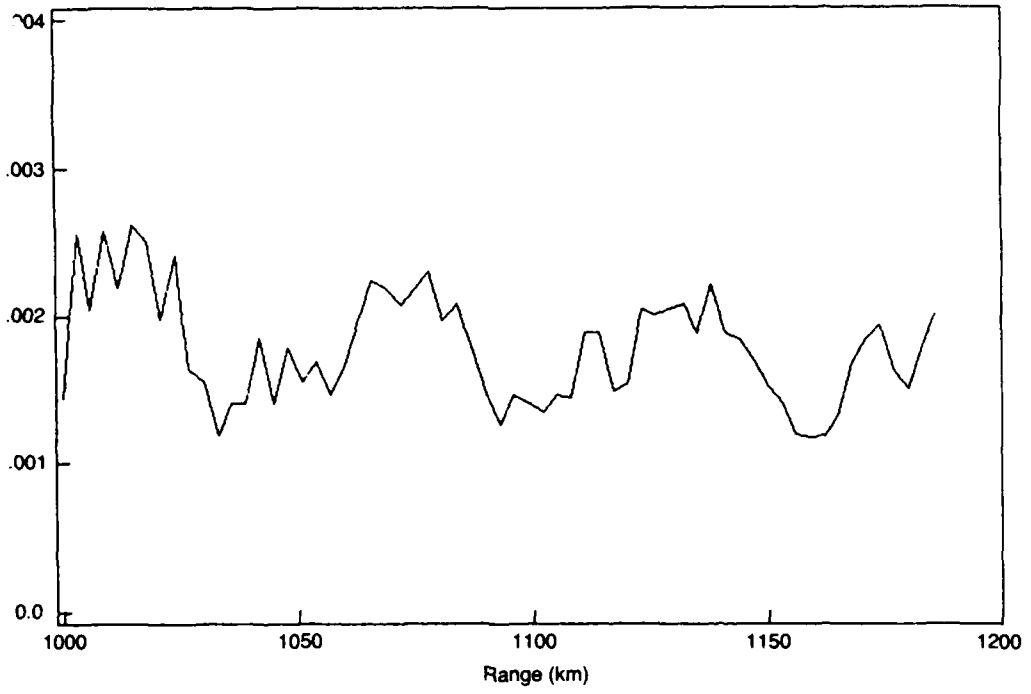


Source: 25 m; Long Range; Shallow Receiver

**Figure 28.** *Information from a dense array between 500 and 1000 m depth.*

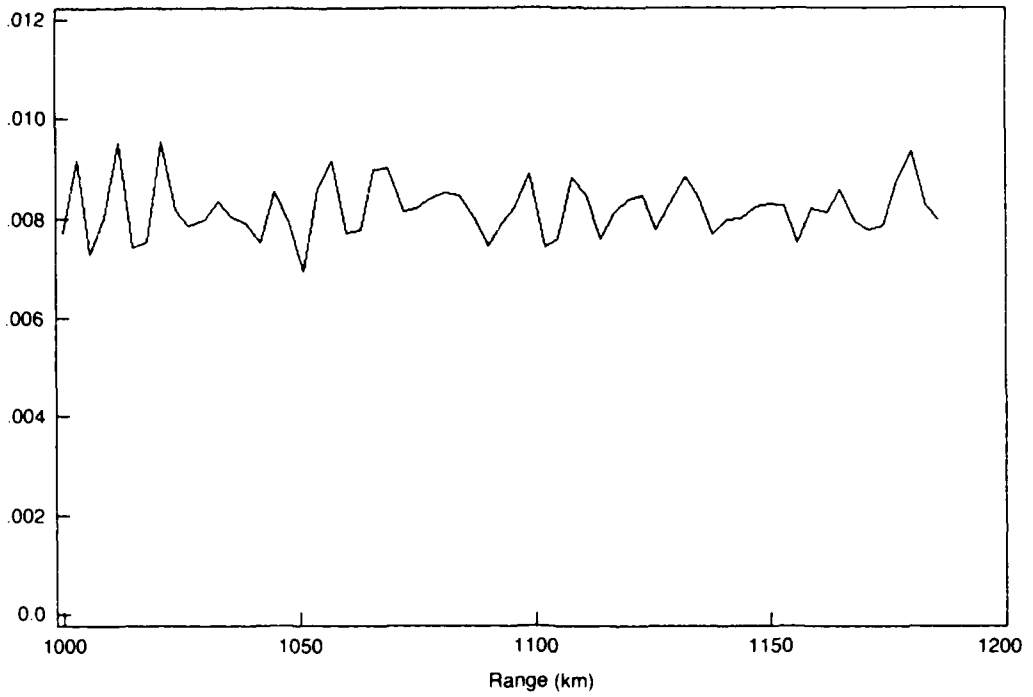


Source: 80 m; Long Range; Shallow Receiver

**Figure 29.** Information from a dense array between 500 and 1000 m depth.

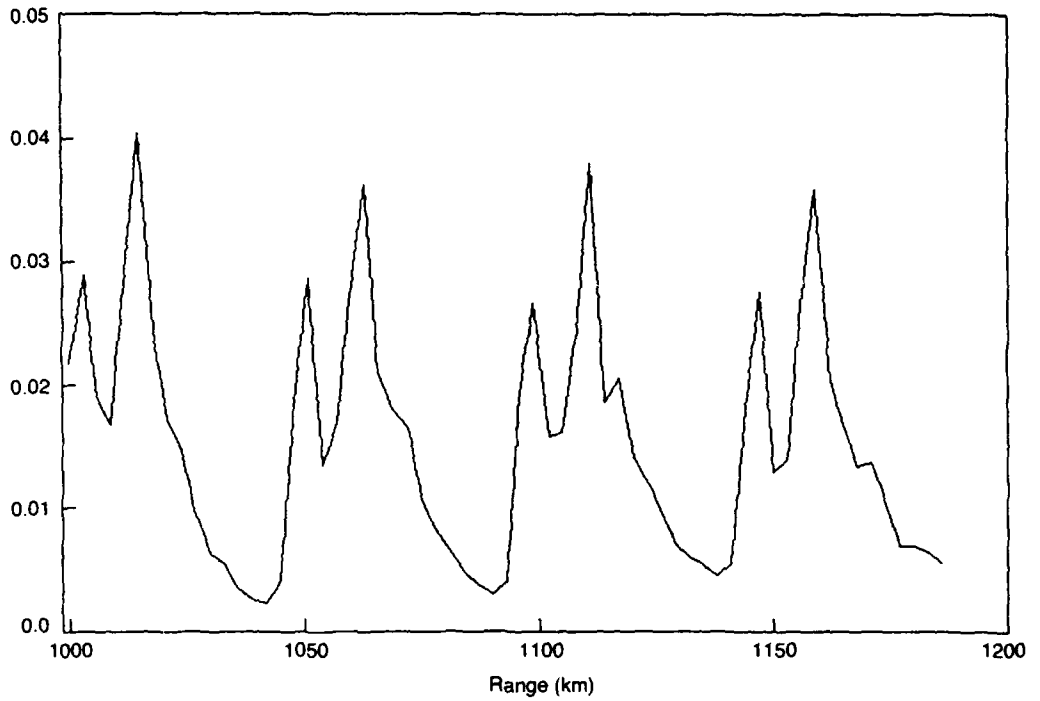


Source: 150 m; Long Range; Shallow Receiver

**Figure 30.** Information from a dense array between 500 and 1000 m depth.

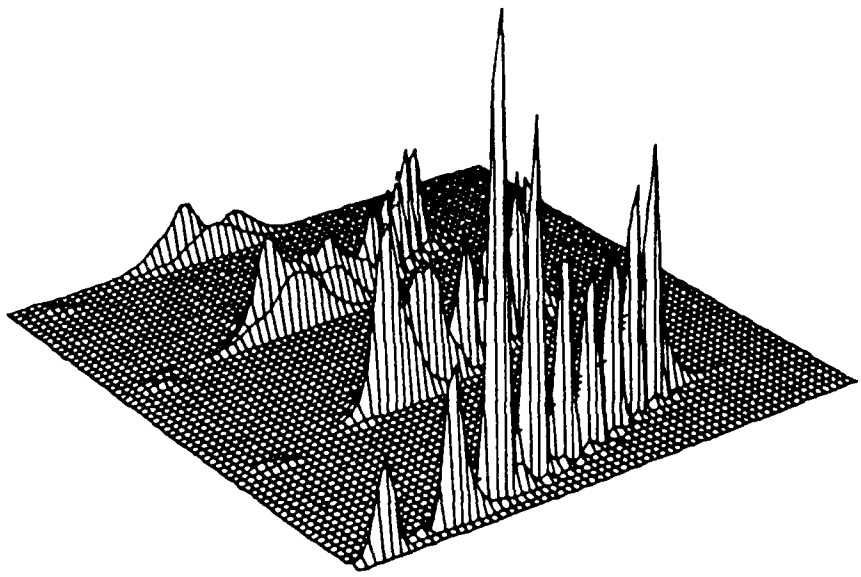

**Figure 31**. Information from a dense array between 3500 and 4000 m depth.

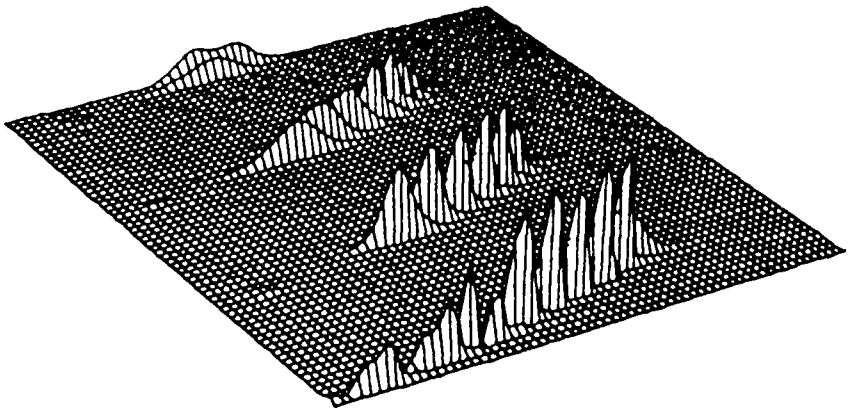

**Figure 32**. Information from a dense array between 3500 and 4000 m depth

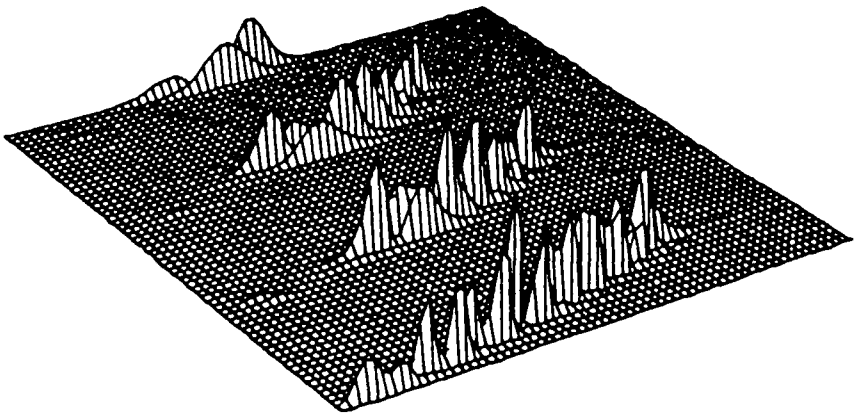

**Figure 33.** Information from a dense array between 3500 and 4000 m depth.

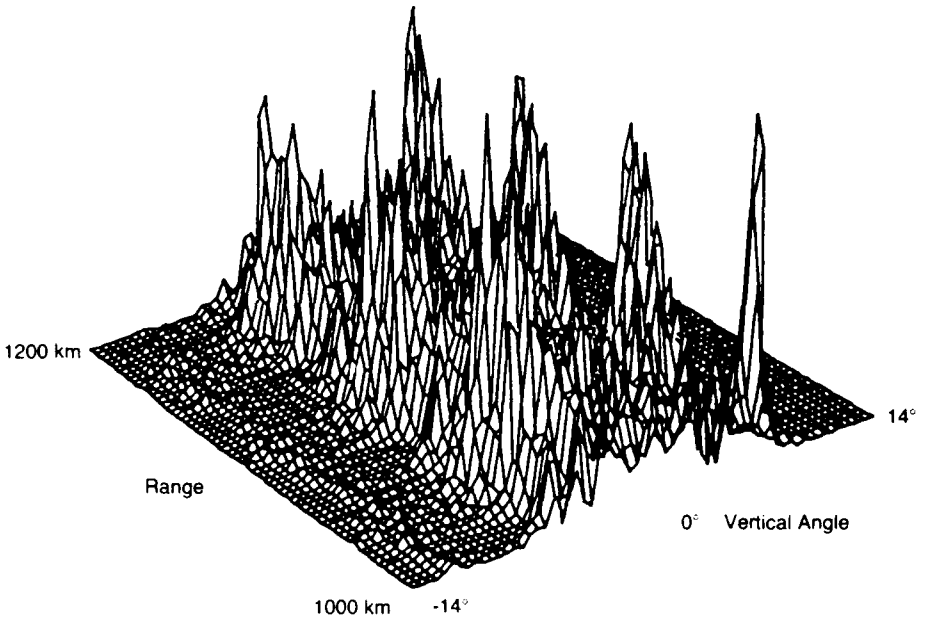


**Figure 34.** Information from a dense array between 3500 and 4000 m depth.

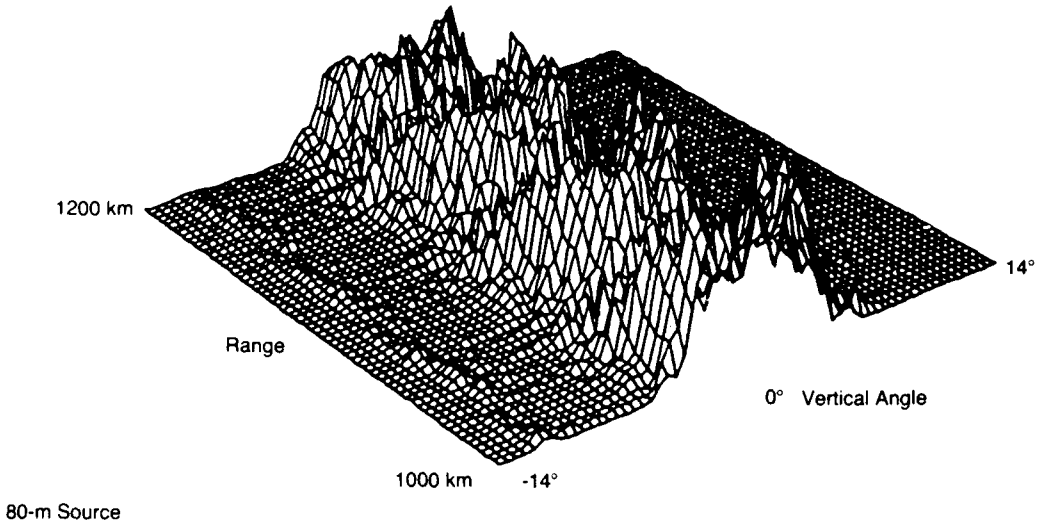


**Figure 35.** Information from a dense array between 3500 and 4000 m depth.

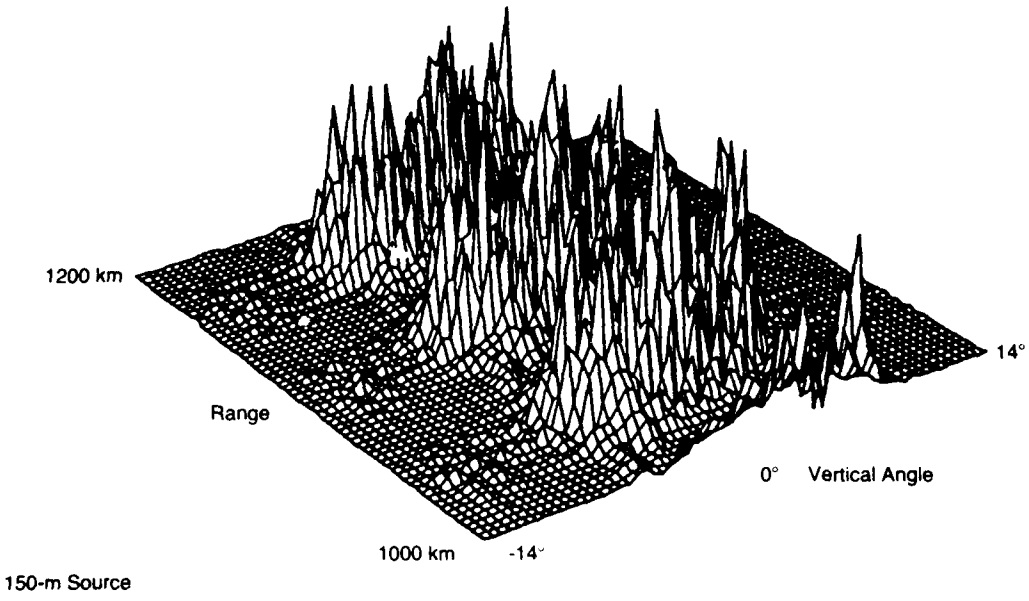


**Figure 36.** Information from a dense array between 3500 and 4000 m depth.

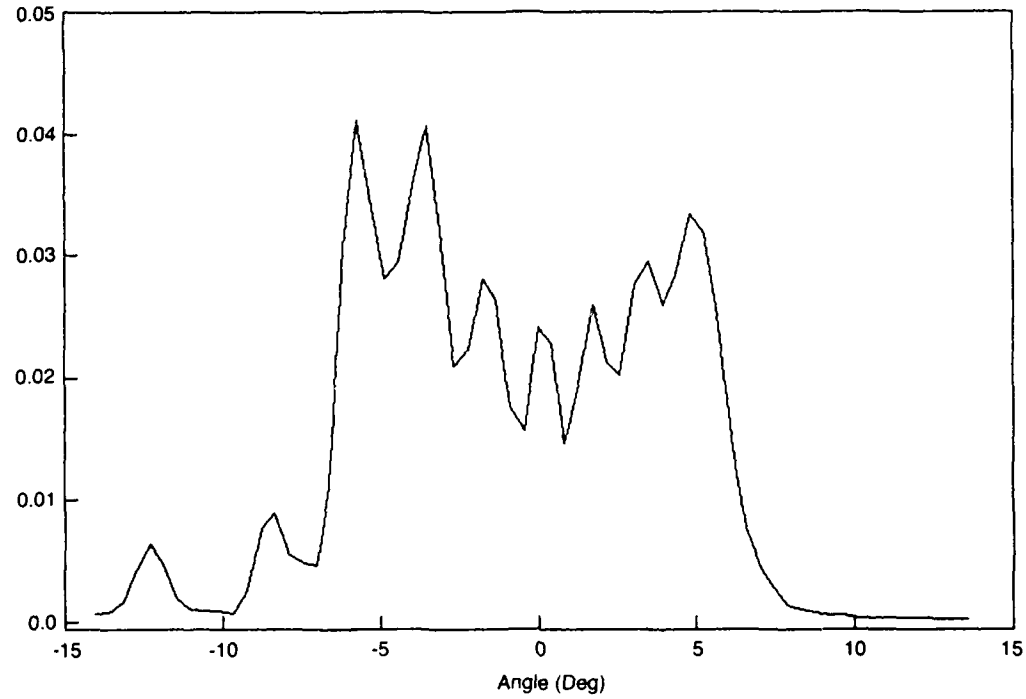


Source: 25 m; Short Range; Deep Receiver

**Figure 37.** Information from a dense array between 3500 and 4000 m depth.

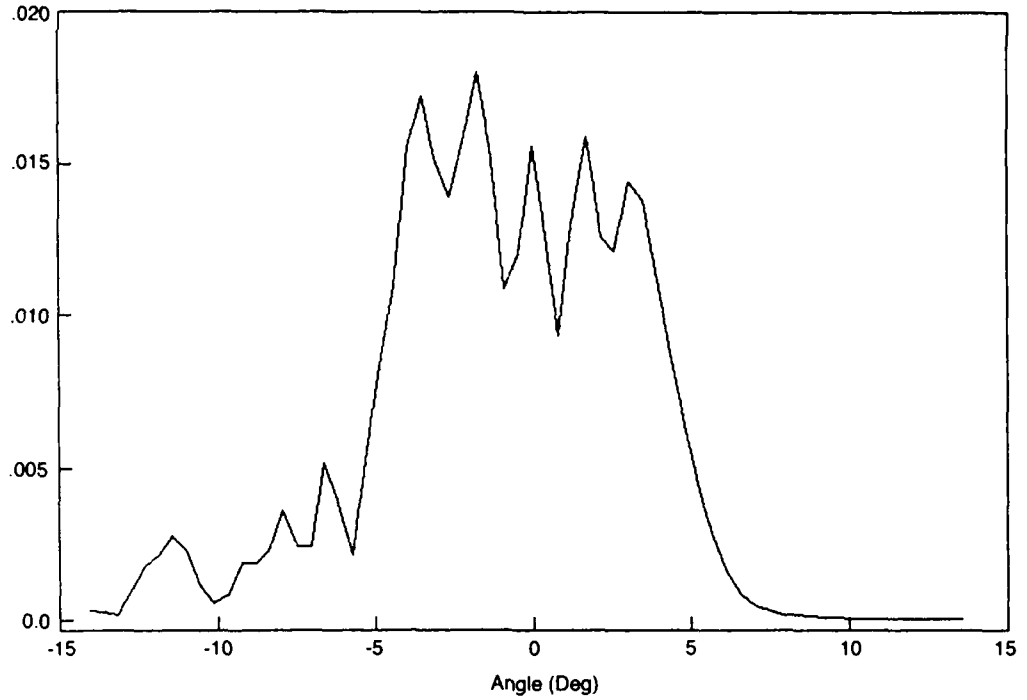


Source: 80 m; Short Range; Deep Receiver

**Figure 38.** Information from a dense array between 3500 and 4000 m depth.

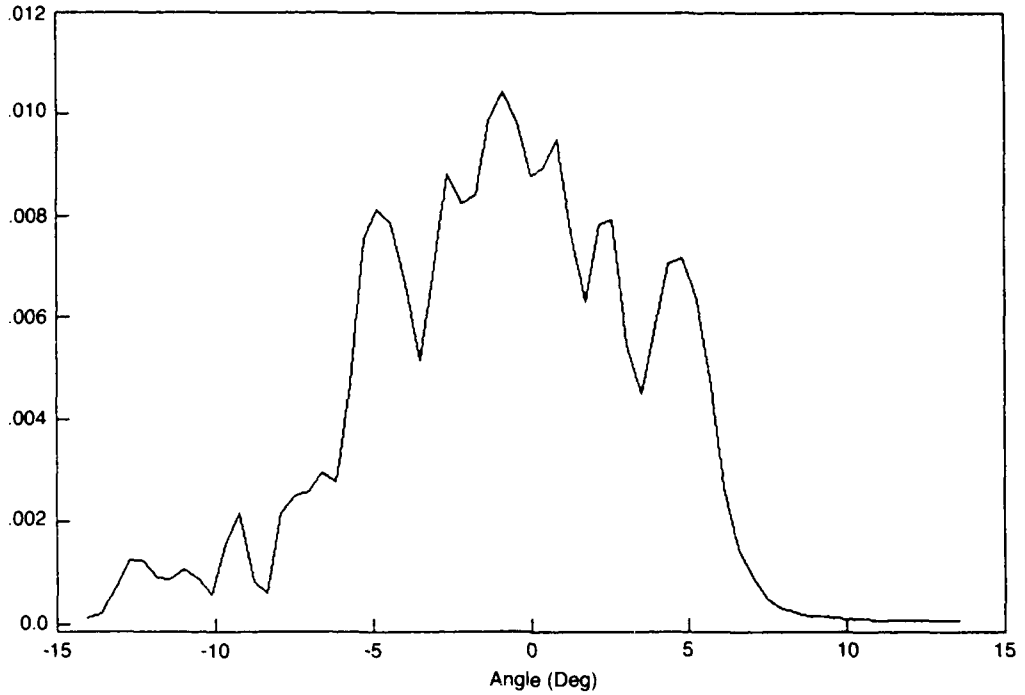


Source: 150 m; Short Range; Deep Receiver

***Figure 39.*** *Information from a dense array between 3500 and 4000 m depth.*

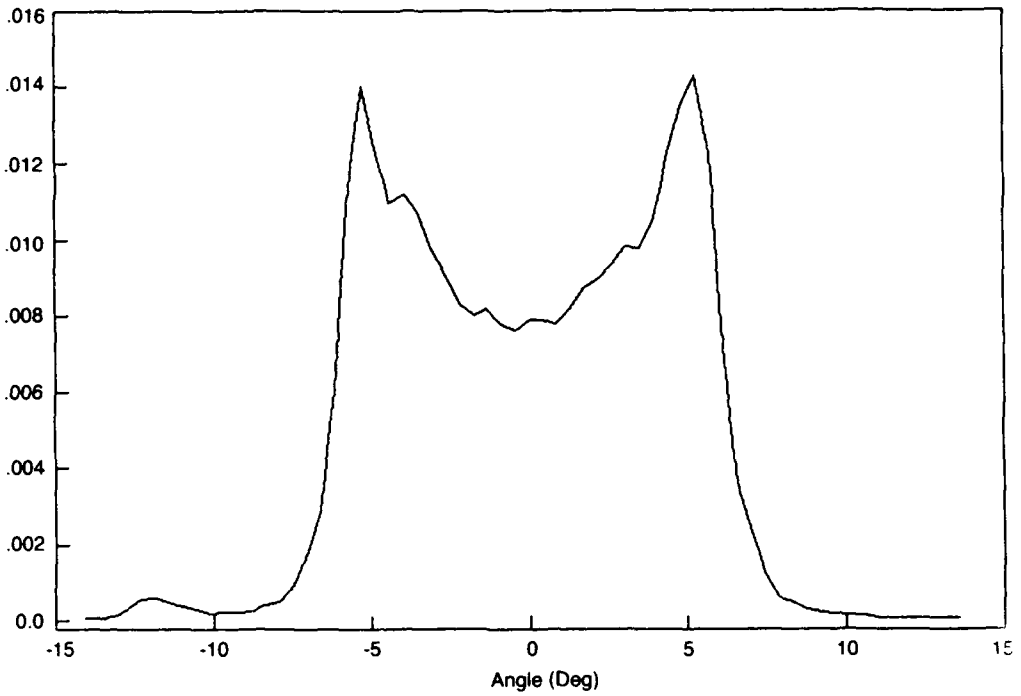


Source: 25 m; Long Range; Deep Receiver

**Figure 40.** Information from a dense array between 3500 and 4000 m depth.

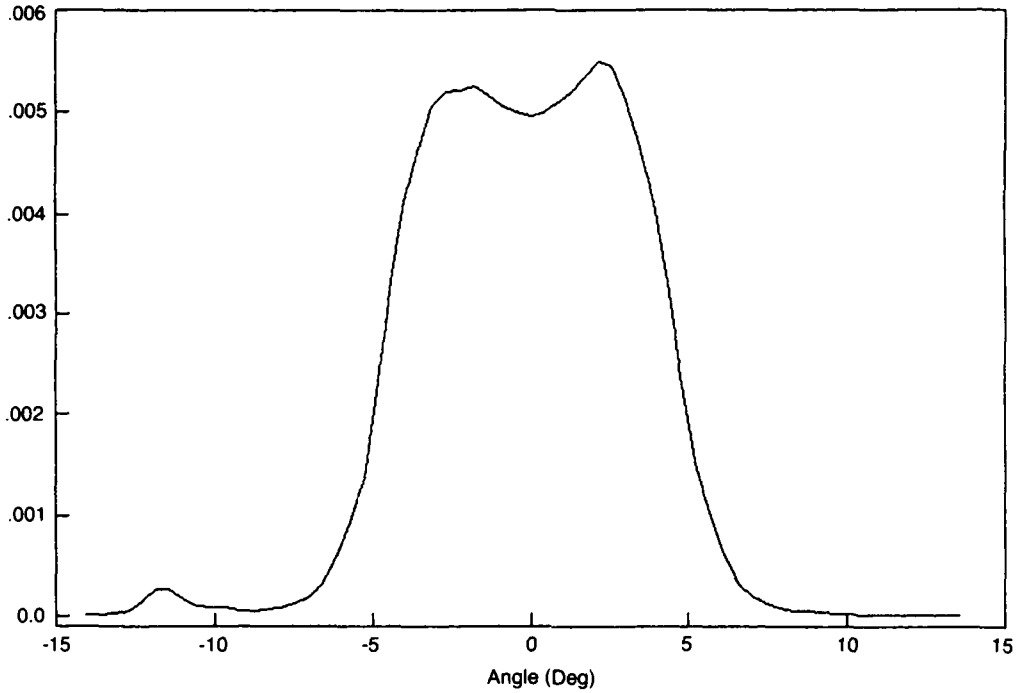


Source: 80 m; Long Range; Deep Receiver

**Figure 41.** *Information from a dense array between 3500 and 4000 m depth.*

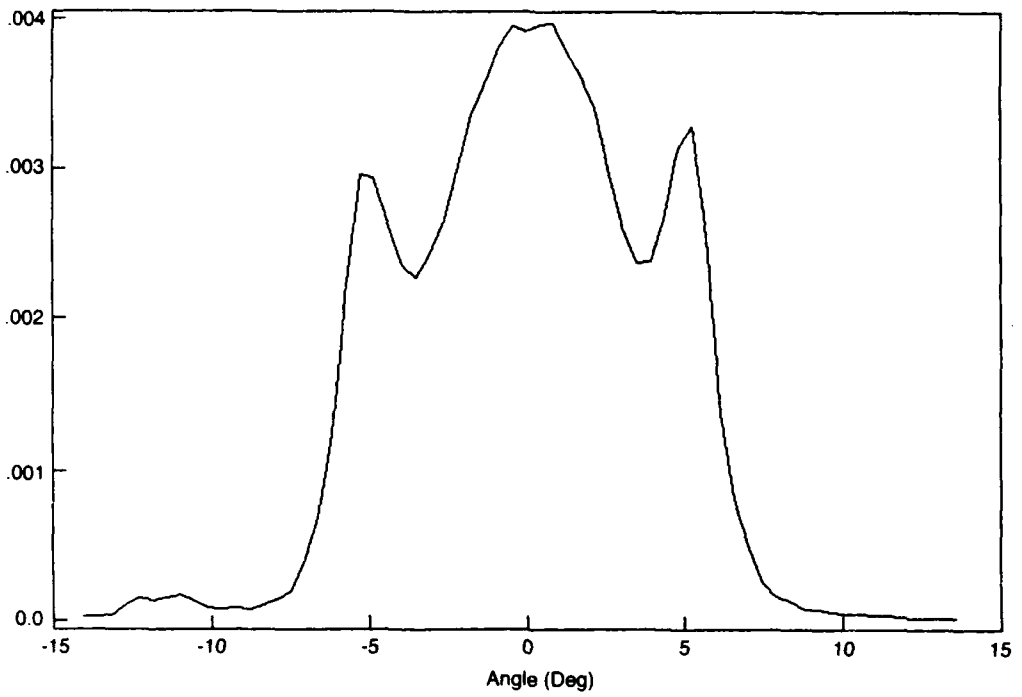


Source: 150 m; Long Range; Deep Receiver

**Figure 42.** Information from a dense array between 3500 and 4000 m depth.

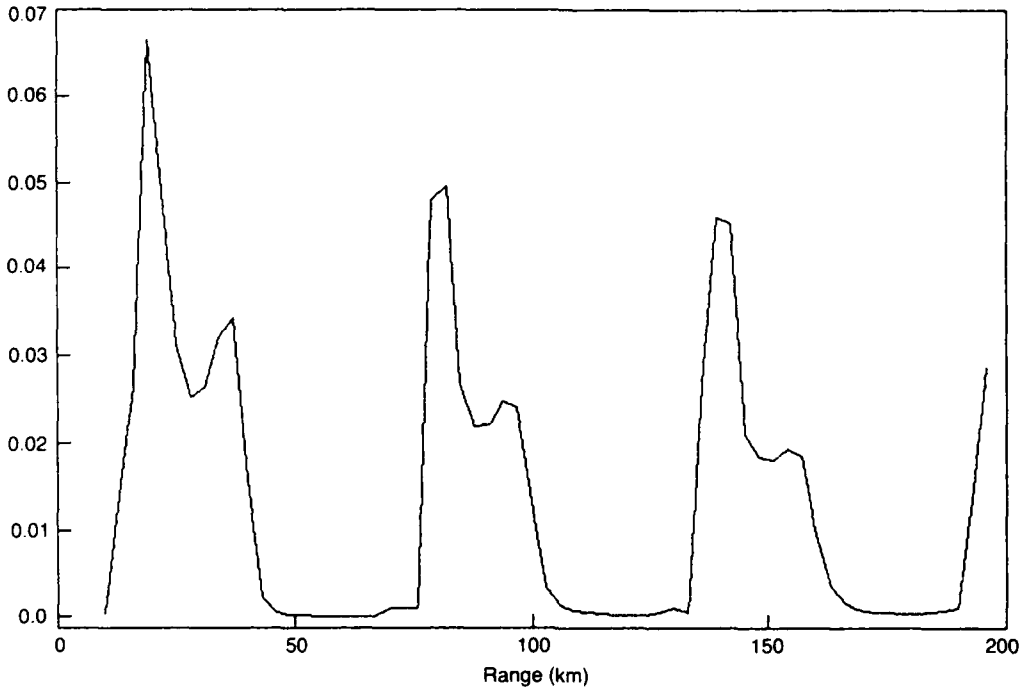


Source: 25 m; Short Range; Deep Receiver

**Figure 43**. Information from a dense array between 3500 and 4000 m depth.

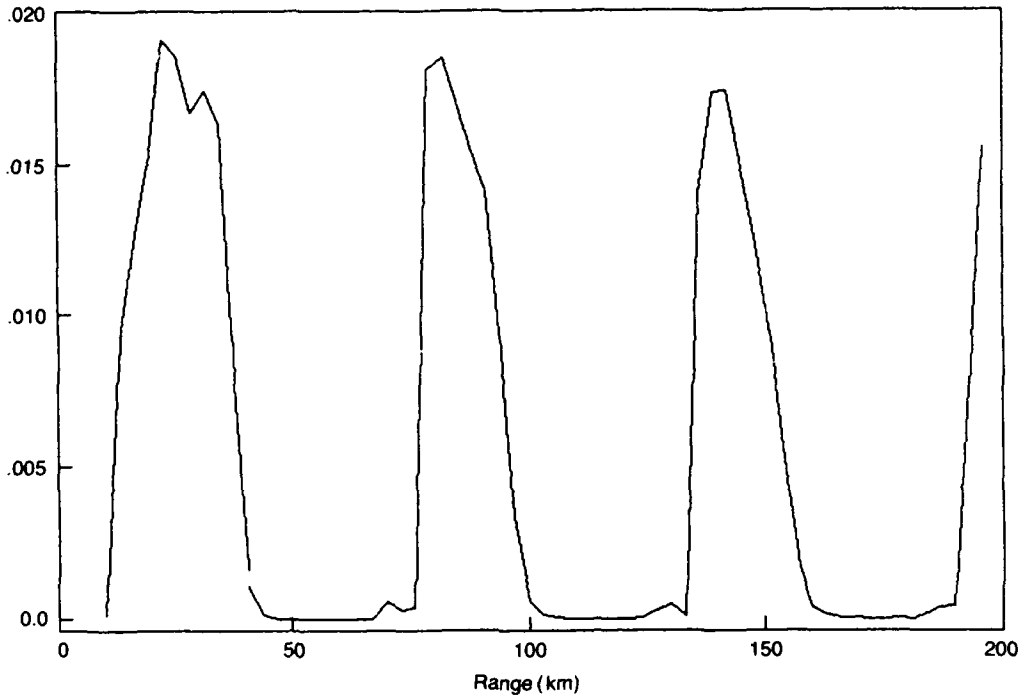


Source: 80 m; Short Range; Deep Receiver

**Figure 44.** Information from a dense array between 3500 and 4000 m depth.

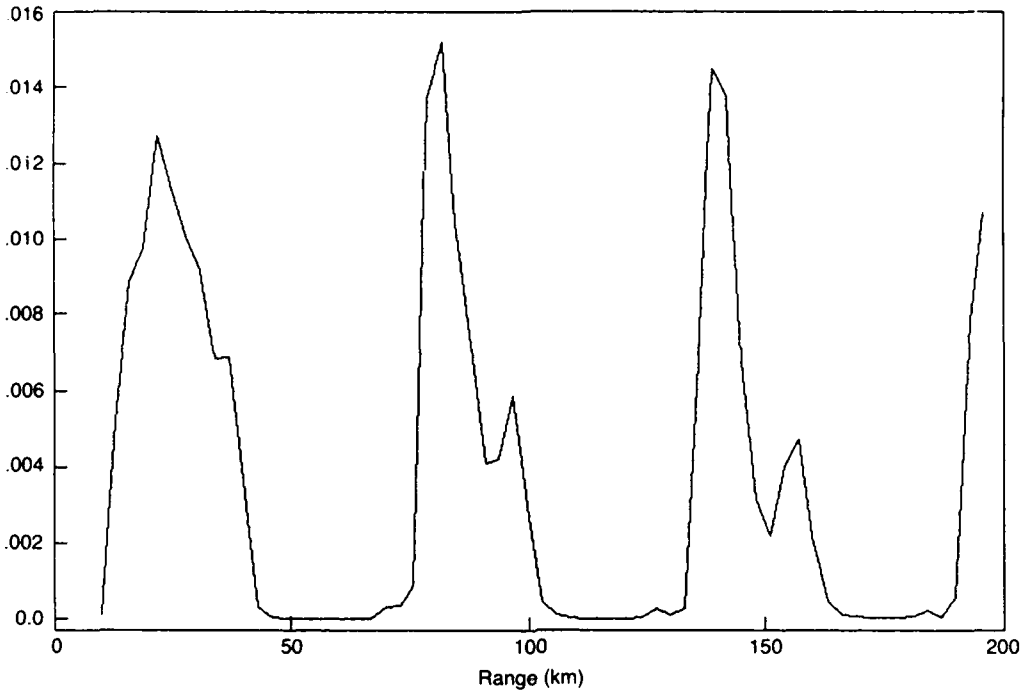


Source: 150 m; Short Range; Deep Receiver

**Figure 45.** Information from a dense array between 3500 and 4000 m depth.

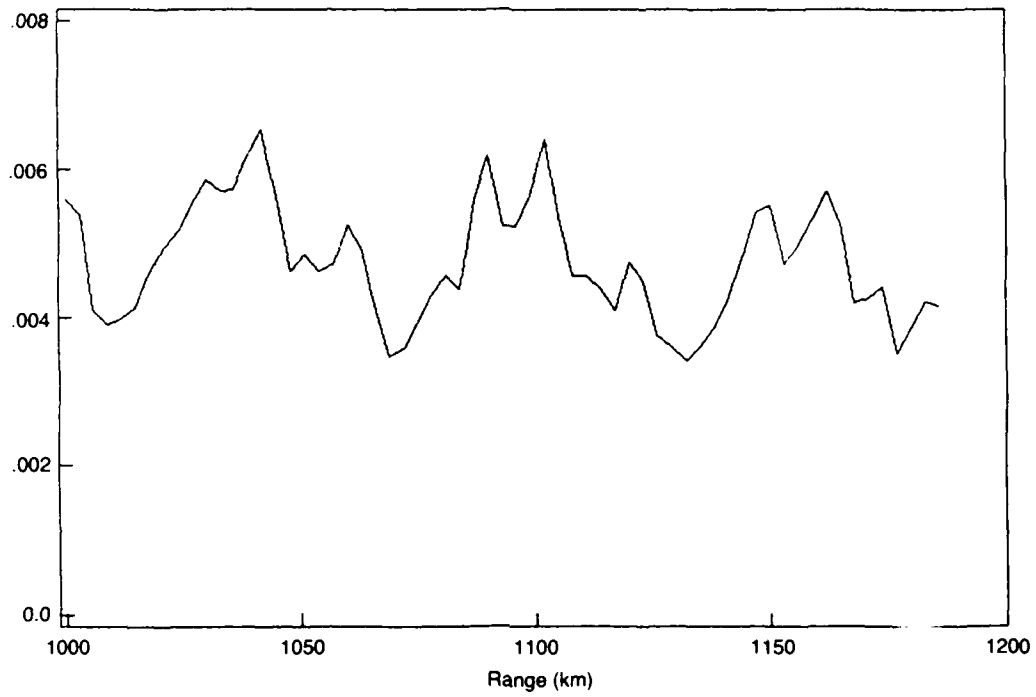


Source: 25 m; Long Range; Deep Receiver

**Figure 46.** Information from a dense array between 3500 and 4000 m depth.

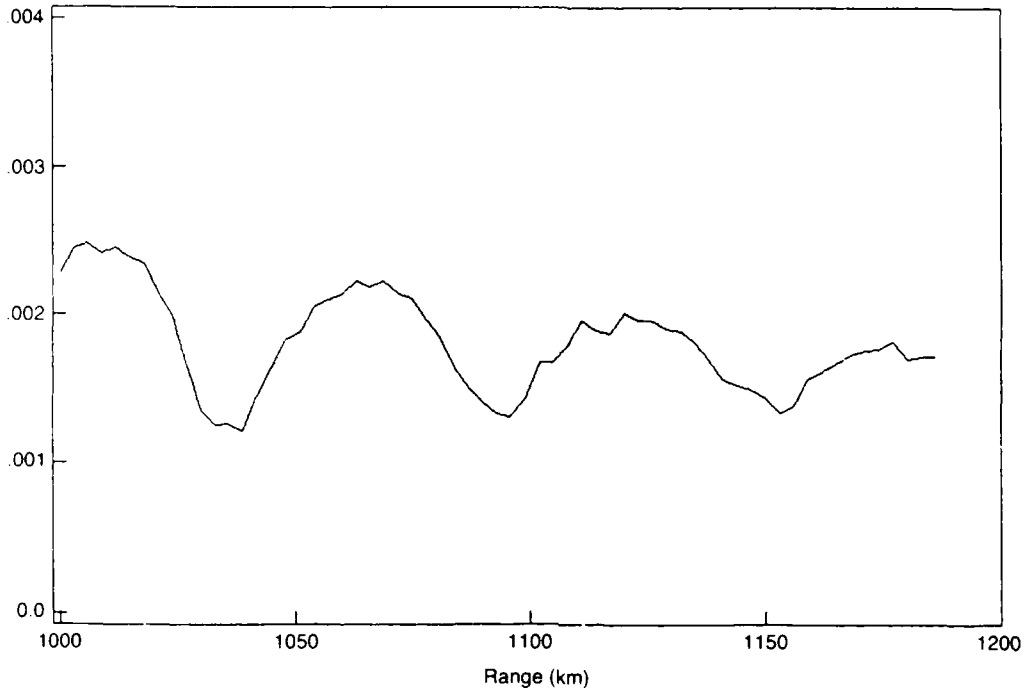


Source: 80 m; Long Range; Deep Receiver

**Figure 47.** Information from a dense array between 3500 and 4000 m depth.

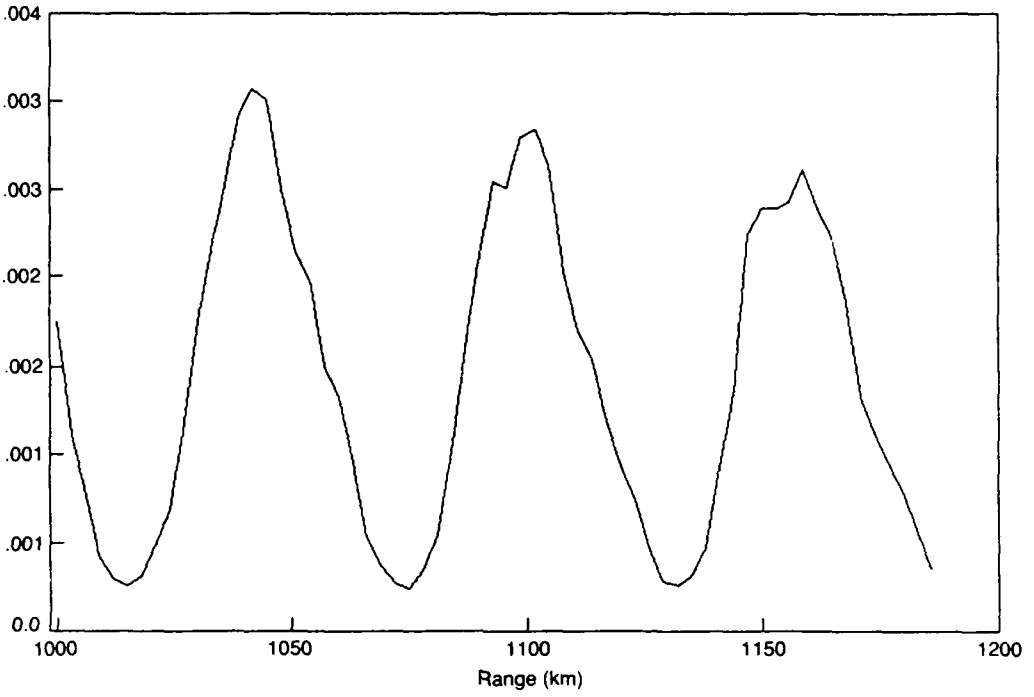


Source: 150 m; Long Range; Deep Receiver

**Figure 48.** *Information from a dense array between 3500 and 4000 m depth.*

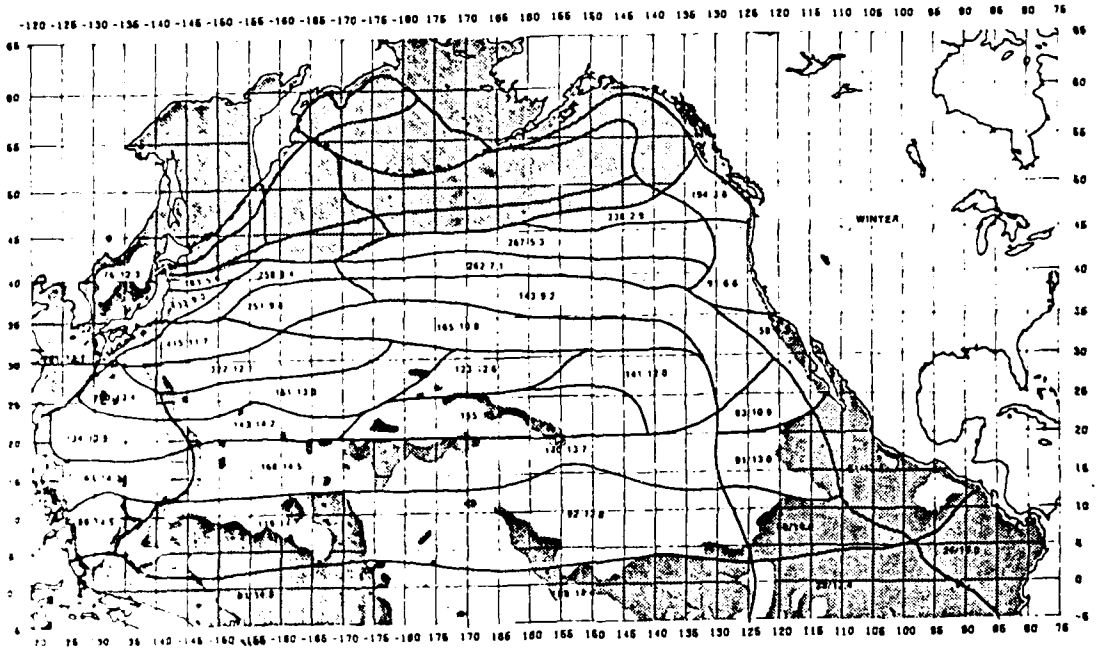


**Figure 49.** Ocean regions. The first number is the depth in feet at which a horizontal ray arrives at the sound channel axis at 1° different angle than the surface limited ray. The second number is the axis angle of the surface-limited array. (See *Reference 3.*)

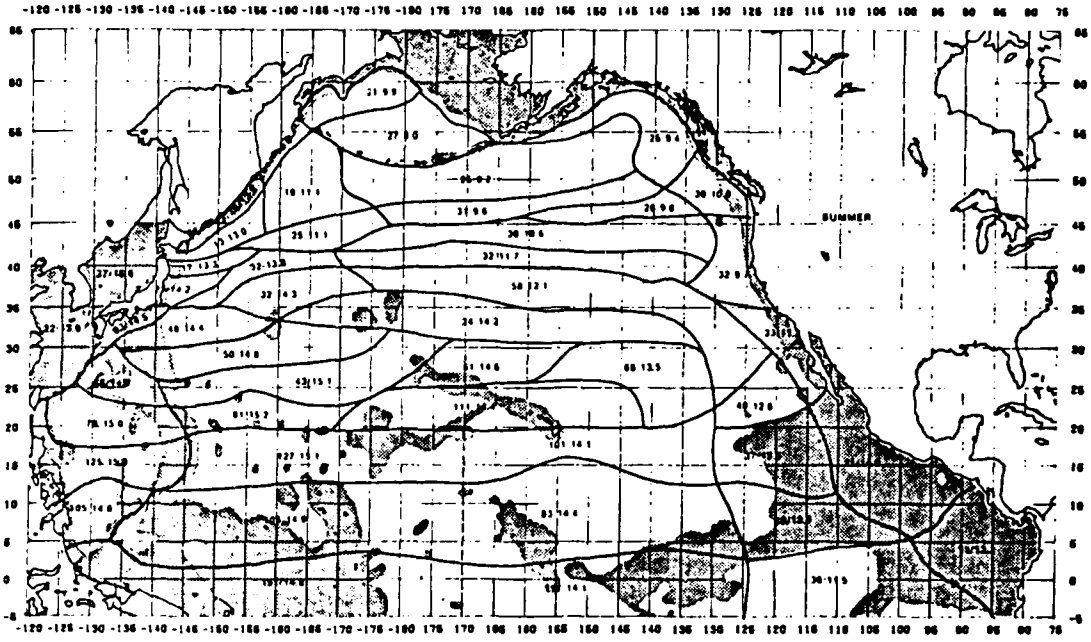


**Figure 50.** Ocean regions. The first number is the depth in feet at which a horizontal ray arrives at the sound channel axis at 1° different angle than the surface limited ray. The second number is the axis angle of the surface-limited array. (See Reference 3.)

## REFERENCES

1. B. Williams and F. Fisher, "Long-range arrival structure", J. Underwater Acoustics, October 1981.

2. B. Williams and F. Fisher, "Extraction of important classification information from a vertical array", J. Underwater Acoustics, October 1982.

3. J. Lovett and X. Wright, "Vertical Array Performance and Applications," Monterey Surveillance Symposium, July 1983.

DISTRIBUTION LIST

Dr. Marv Atkins
Deputy Director, Science & Tech.
Defense Nuclear Agency
Washington, D.C. 20305

National Security Agency
Attn RS: Dr. N. Addison Ball
Ft. George G. Meade, MD 20755

Dr. Robert Cooper [2]
Director, DARPA
1400 Wilson Boulevard
Arlington, VA 22209

Defense Technical Information [2]
Center
Cameron Station
Alexandria, VA 22314

The Honorable Richard DeLauer
Under Secretary of Defense (R&E)
Office of the Secretary of
Defense
The Pentagon, Room 3E1006
Washington, D.C. 20301

Director [2]
National Security Agency
Fort Meade, MD 20755
ATTN: Mr. Richard Foss, A05

CAPT Craig E. Dorman
Department of the Navy, OP-095T
The Pentagon, Room 5D576
Washington, D.C. 20350

CDR Timothy Dugan
NFOIO Detachment, Suitland
4301 Suitland Road
Washington, D.C. 20390

Dr. Larry Gershwin
NIO for Strategic Programs
P.O. Box 1925
Washington, D.C. 20505

Dr. S. William Gouse, W300
Vice President and General
Manager
The MITRE Corporation
1820 Dolley Madison Blvd.
McLean, VA 22102

Dr. Edward Harper
SSBN, Security Director
OP-021T
The Pentagon, Room 4D534
Washington, D.C. 20350

Mr. R. Evan Hineman
Deputy Director for Science
& Technology
P.O. Box 1925
Washington, D.C 20505

Mr. Ben Hunter [2]
CIA/DDS&T
P.O. Box 1925
Washington, D.C. 20505

The MITRE Corporation [25]
1820 Dolley Madison Blvd.
McLean, VA 22102
ATTN: JASON Library, W002

Mr. Jack Kalish
Deputy Program Manager
The Pentagon
Washington, D.C. 20301

Mr. John F. Kaufmann
Dep. Dir. for Program Analysis
Office of Energy Research, ER-31
Room F326
U.S. Department of Energy
Washington, D.C. 20545

Distribution List
continued

Dr. George A. Keyworth
Director
Office of Science & Tech. Policy
Old Executive Office Building
17th & Pennsylvania, N.W.
Washington, D.C. 20500

MAJ GEN Donald L. Lamberson
Assistant Deputy Chief of Staff
(RD&A) HQ USAF/RD
Washington, D.C. 20330

Dr. Donald M. LeVine, W385 [3]
The MITRE Corporation
1820 Dolley Madison Blvd.
McLean, VA 22102

Mr. V. Larry Lynn
Deputy Director, DARPA
1400 Wilson Boulevard
Arlington, VA 22209

Dr. Joseph Mangano [2]
DARPA/DEO
9th floor, Directed Energy Office
1400 Wilson Boulevard
Arlington, VA 22209

Mr. John McMahon
Dep. Dir. Cen. Intelligence
P.O. Box 1925
Washington, D.C. 20505

Director
National Security Agency
Fort Meade, MD 20755
ATTN: William Mehuron, DDR

Dr. Marvin Moss
Technical Director
Office of Naval Research
800 N. Quincy Street
Arlington, VA 22217

Dr. Julian Nall [2]
P.O. Box 1925
Washington, D.C. 20505

Director
National Security Agency
Fort Meade, MD 20755
ATTN: Mr. Edward P. Neuburg
DDR-FANX 3

Prof. William A. Nierenberg
Scripps Institution of
Oceanography
University of California, S.D.
La Jolla, CA 92093

Mr. C. Wayne Peale
Office of Research and
Development
P.O. Box 1925
Washington, DC 20505

The MITRE Corporation
Records Resources
Mail Stop W971
McLean, VA 22102

Mr. Alan J. Roberts
Vice President & General Manager
Washington $C^3$ Operations
The MITRE Corporation
1820 Dolley Madison Boulevard
Box 208
McLean, VA 22102

Los Alamos Scientific Laboratory
ATTN: C. Paul Robinson
P.O. Box 1000
Los Alamos, NM 87545

Mr. Richard Ross [2]
P.O. Box 1925
Washington, D.C. 20505

Distribution List
concluded

Dr. Phil Selwyn
Technical Director
Office of Naval Technology
800 N. Quincy Street
Arlington, VA 22217

Dr. Eugene Sevin [2]
Defense Nuclear Agency
Washington, D.C. 20305

Mr. Robert Shuckman
P.O. Box 8618
Ann Arbor, MI 48107

Dr. Joel A. Snow [2]
Senior Technical Advisor
Office of Energy Research
U.S. DOE, M.S. E084
Washington, D.C. 20585

Mr. Alexander J. Tachmindji
Senior Vice President & General
Manager
The MITRE Corporation
P.O. Box 208
Bedford, MA 01730

Dr. Vigdor Teplitz
ACDA
320 21st Street, N.W.
Room 4484
Washington, D.C. 20451

Dr. Al Trivelpiece
Director, Office of Energy
Research, U.S. DOE
M.S. 6E084
Washington, D.C. 20585

Mr. James P. Wade, Jr.
Prin. Dep. Under Secretary of
Defense for R&E
The Pentagon, Room 3E1014
Washington, D.C. 20301

Mr. Leo Young
OUSDRE (R&AT)
The Pentagon, Room 3D1067
Washington, D.C. 20301

# END

# FILMED

3-85

# DTIC